Response to Reviewer #1

## Technical comments:

**Q1**- I was not implying that the sCIs themselves form SOA. Rather I was speculating on the role of sCIs to oxidize SOA precursors to form SOA. Nonetheless, the response and the conclusions in the paper about evidence for acid-catalyzed reactions is weak and needs to be revised even further.

Reply: $CH_2OO$ and $CH_3CHOO$ were the main sCIs in this study and there is still no evidence that these sCIs can oxidize SOA precursors to form SOA. If sCIs directly oxidized SOA precursors and formed substantial SOA, the presence of high concentration of $SO_2$ would consume sCIs and thus decrease the formation of SOA. However, higher SOA production was observed for experiments with the addition of $SO_2$, indicating that sCIs formed during the photo-oxidation of gasoline vehicle exhaust might not directly oxidize SOA precursors to form substantial SOA. This also ruled out the possibility of enhanced gas-phase chemistry. As the fragment m/z 88 can only arise from glyoxal oligomer formed through acid-catalyzed reactions, the higher intensity of m/z 88 under higher acidity condition was an important evidence for acid-catalyzed reactions. Two smooth solid lines, based on the average values of every five data points, were added into the revised Figure 9 to highlight the higher intensity of m/z 88 for the experiment with the addition of $SO_2$. The low intensities of m/z 88 do not indicate that oligomers formed from glyoxal are not important. It is more likely that these fragments are thermally unstable at the vaporization temperature of AMS (600 ℃) and readily decompose to monomer or *gem*-diol forms before entering the ionization region. Additionally, the significant correlation between particle acidity and SOA production factors also indicated the important role of acid-catalyzed reactions, since the effect of sulfate on SOA formation was ruled out through seeded experiments.

The following text "*Fig. 9 shows the ion intensity of fragment m/z 88 that can arise only from a glyoxal oligomer (Liggio et al., 2015). The scatter of the data might be due to the low intensity of m/z 88. However, the experiment …*" has been changed to

"Fig. 9 shows the ion intensity of fragment m/z 88 that can arise only from a glyoxal oligomer formed through acid-catalyzed heterogeneous reactions (Liggio et al., 2015). The scatter of the data might be due to the low intensity of m/z 88. The low intensities of m/z 88 may not indicate that oligomers formed from glyoxal are not important. It is more likely that these fragments are thermally unstable at the vaporization temperature of HR-TOF-AMS (600 ℃) and readily decompose to monomer or *gem*-diol forms before passing into the ionization region. The experiment…"

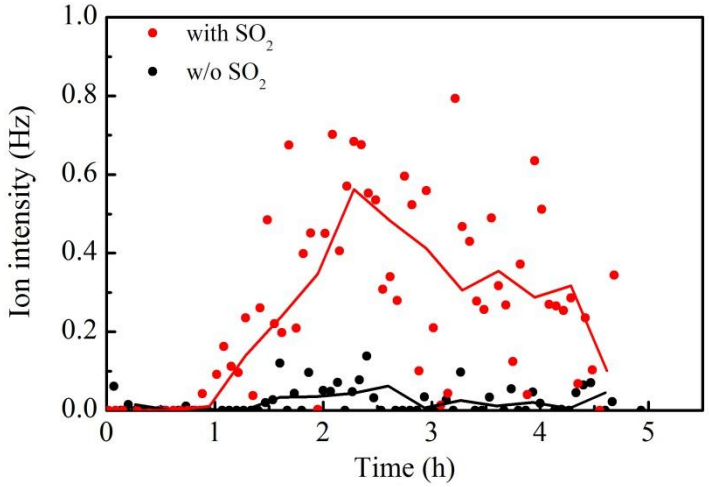


**Q2-** I am confused by the interpretation offered by the authors based on results of the new experiment. Ammonium sulfate at 59% RH should be a solid. The experiment has merely tested the availability of a condensation sink on SOA formation; it's nice to see that the experiments are not surface area limited. However, the experiment says nothing about whether the SOA enhancement is a result of increased acidity. The experiment that should have been performed, in my opinion, is with wet aerosol to test the role of acidity and rule out the possibility of enhanced gas-phase chemistry.

Reply: The new experiment was conducted to explore the effect of sulfate and vapor wall loss on SOA formation. Thus the RH was kept comparable with that in experiment I-1. As addressed in Q1, the higher intensity of m/z 88 under higher acidity condition and significant correlation between particle acidity and SOA production factors demonstrated the important role of acid-catalyzed reactions. The possibility of enhanced gas-phase chemistry is also addressed in Q1.

**Q3-** I do not think the authors have offered a correct explanation of the influence of

vapor wall-losses on these set of experiments. Zhang et al. (2014) see a large influence of wall losses on SOA production not from the loss of the 'final' semi-volatile product species but because of the loss of intermediary (potentially intermediate volatility) species that are lost to the walls before they form SOA.

Reply: The explanation referring to partitioning coefficients may be confusing. This part will be deleted in the revised manuscript. Comparable SOA PFs for experiments with and without seed aerosols observed in this study indicated that wall loss of organic vapors did not significantly impact SOA production from gasoline vehicle exhaust.

The following text has been deleted in the revised manuscript.

"*The addition of $SO_2$ may vary the vapor wall loss rate and influence the estimation of SOA production. The wall accommodation coefficient ($\alpha_{w,i}$), governing the extent of wall deposition of a compound i, was observed to be inversely dependent on its effective saturation concentration $C_i^*$ (X. Zhang et al., 2015). Partitioning coefficients for different $C_i^*$ ranging from 0.01 to $10^6$ $\mu g\ m^{-3}$ were calculated using gas-particle partitioning theory (Donahue et al., 2006) (Table 6). Partitioning coefficients for experiments with and without the addition of $SO_2$ mainly exhibited big differences for $C_i^*$ bins of 10 and 100 $\mu g\ m^{-3}$ with $\alpha_{w,i}$ calculated to be $3.1\times10^{-7}$ and $2.0\times10^{-7}$, respectively. The wall loss rate for $C_i^*$ bin of 10 $\mu g\ m^{-3}$ would then be approximately 50% higher than that for $C_i^*$ bin of 100 $\mu g\ m^{-3}$ assuming a linear relation between wall loss rate and $\alpha_{w,i}$ (X. Zhang et al., 2015). An increase of 50% in wall loss rate would lead to 11.5% higher vapor loss to walls when assuming the wall loss rate to be $2.0\times10^{-5}$ $s^{-1}$, similar to a product of the photo-oxidation of toluene. Thus, biases of vapor wall loss rates due to the addition of $SO_2$ may have negligible influence on estimation of SOA production.*"

The following text "*However, comparable SOA PFs for experiments with and without seed aerosols observed in this study indicated the negligible impact of seed aerosols on SOA production. Cocker III et al. (2001) also observed that the presence of ammonium sulfate seed aerosols had no impact on SOA formation from the photo-oxidation of m-xylene and 1,3,5-trimethylbenzene.*" has been changed to

"However, Cocker III et al. (2001) observed that the presence of ammonium sulfate seed aerosols had no impact on SOA formation from the photo-oxidation of m-xylene and 1,3,5-trimethylbenzene. Li et al. (2015) also suggested that no measurable differences were observed in SOA formation from m-xylene between non-seeded and seeded experiments. In this study, comparable SOA PFs for experiments with and without seed aerosols indicated wall loss of organic vapors did not significantly impact SOA production from gasoline vehicle exhaust."

**Q4-** In the introduction, the manuscript would benefit from the hypotheses surrounding the poor model-measurement comparison of SOA from light-duty gasoline vehicles.

Reply: The following text has been added to the introduction section.

"Multiple studies have shown that modeled SOA can only explain a fraction of the measured SOA from gasoline vehicle exhaust (Platt et al., 2013; Tkacik et al., 2014). Platt et al. (2013) found that predicted SOA accounted for approximately 20% of the SOA formed from Euro 5 gasoline vehicle exhaust. Hence, more studies are needed to bridge the gap between modeled and measured SOA from gasoline vehicle exhaust."

**Q5-** I am concerned that the experiment includes passing emissions through a pump where depending on the pump type, you could get substantial loss of gas and particle species on the impeller/diaphragm. On a related note, have the authors performed blanks to look at SOA formation in the absence of emissions?

Reply: This issue has been addressed in our previous paper (Liu et al., 2015). Losses of particles and VOCs in the introduction system were determined by comparing the concentrations of total particle number and VOCs in the directly emitted exhaust and the ones after passing through the transfer system. The loss of total particle number and VOCs was estimated to be less than 3% and 5%, respectively. As the same pump was used to introduce vehicle exhaust into the reactor for experiments with and without the addition of $SO_2$, we concluded that the loss of gas and particle species in the introduction system would not affect the major conclusions in this study. Blank experiments with no vehicle exhaust introduced were performed to quantify the reactivity of the matrix gas. After 5 h of irradiation, the number and mass of formed

particles were <5 $cm^{-3}$ and 0.1 μg $m^{-3}$, respectively. Particle number distribution in a blank experiment was shown.

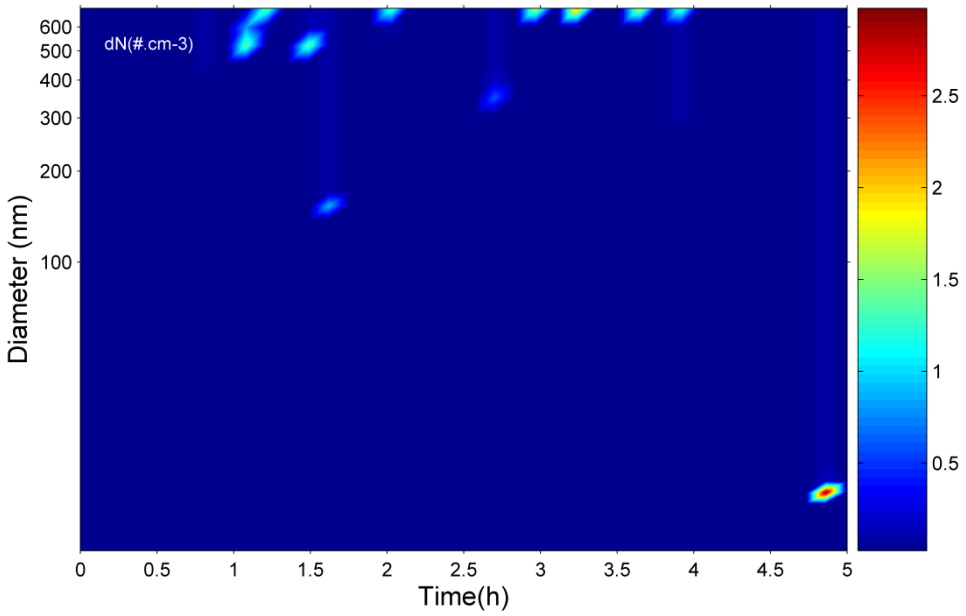


**References**

Li, L., Tang, P., and Cocker Iii, D. R.: Instantaneous nitric oxide effect on secondary organic aerosol formation from m-xylene photooxidation, Atmos. Environ., 119, 144-155, doi:10.1016/j.atmosenv.2015.08.010, 2015.

Liu, T., Wang, X., Deng, W., Hu, Q., Ding, X., Zhang, Y., He, Q., Zhang, Z., Lü, S., Bi, X., Chen, J., and Yu, J.: Secondary organic aerosol formation from photochemical aging of light-duty gasoline vehicle exhausts in a smog chamber, Atmos. Chem. Phys., 15, 9049-9062, 10.5194/acp-15-9049-2015, 2015.

Platt, S. M., El Haddad, I., Zardini, A. A., Clairotte, M., Astorga, C., Wolf, R., Slowik, J. G., Temime-Roussel, B., Marchand, N., Ježek, I., Drinovec, L., Močnik, G., Möhler, O., Richter, R., Barmet, P., Bianchi, F., Baltensperger, U., and Prévôt, A. S. H.: Secondary organic aerosol formation from gasoline vehicle emissions in a new mobile environmental reaction chamber, Atmos. Chem. Phys., 13, 9141-9158, doi:10.5194/acp-13-9141-2013, 2013.

Tkacik, D. S., Lambe, A. T., Jathar, S., Li, X., Presto, A. A., Zhao, Y. L., Blake, D., Meinardi, S., Jayne, J. T., Croteau, P. L., and Robinson, A. L.: Secondary Organic Aerosol Formation from in-Use Motor Vehicle Emissions Using a Potential Aerosol

Mass Reactor, Environ. Sci. Technol., 48, 11235-11242, doi:10.1021/es502239v, 2014.

Response to Reviewer #3

## General comments:

The authors have made substantial changes to improve the manuscript. They seemed to have addressed the comments made by each reviewer. Nonetheless, the manuscript still requires some minor revisions before it is ready for final publication.

## Specific comments:

**Q1**-Table 6 and lines 405-426 refer to "partitioning coefficients." I am unfamiliar with the term, and therefore this section was confusing. My best guess is that the values in the table correspond to the expected condensed phase mass fraction for organic material in each C* bin. If that is the case, Table 6 has much less to do with wall losses than it does with Coa (total organic aerosol concentration) and partitioning.

Reply: The explanation referring to partitioning coefficients may be confusing. This part will be deleted in the revised manuscript. Comparable SOA PFs for experiments with and without seed aerosols observed in this study indicated that wall loss of organic vapors did not significantly impact SOA production from gasoline vehicle exhaust.

The following text has been deleted in the revised manuscript.

"*The addition of $SO_2$ may vary the vapor wall loss rate and influence the estimation of SOA production. The wall accommodation coefficient ($\alpha_{w,i}$), governing the extent of wall deposition of a compound i, was observed to be inversely dependent on its effective saturation concentration $C_i^*$ (X. Zhang et al., 2015). Partitioning coefficients for different $C_i^*$ ranging from 0.01 to $10^6$ $\mu g\ m^{-3}$ were calculated using gas-particle partitioning theory (Donahue et al., 2006) (Table 6). Partitioning coefficients for experiments with and without the addition of $SO_2$ mainly exhibited big differences for $C_i^*$ bins of 10 and 100 $\mu g\ m^{-3}$ with $\alpha_{w,i}$ calculated to be $3.1\times10^{-7}$ and $2.0\times10^{-7}$, respectively. The wall loss rate for $C_i^*$ bin of 10 $\mu g\ m^{-3}$ would then be approximately 50% higher than that for $C_i^*$ bin of 100 $\mu g\ m^{-3}$ assuming a linear relation between wall loss rate and $\alpha_{w,i}$ (X. Zhang et al., 2015). An increase of 50% in wall loss rate would lead to 11.5% higher vapor loss to walls when assuming the wall*

*loss rate to be 2.0×10$^{-5}$ s$^{-1}$, similar to a product of the photo-oxidation of toluene. Thus, biases of vapor wall loss rates due to the addition of $SO_2$ may have negligible influence on estimation of SOA production.*"

The following text "*However, comparable SOA PFs for experiments with and without seed aerosols observed in this study indicated the negligible impact of seed aerosols on SOA production. Cocker III et al. (2001) also observed that the presence of ammonium sulfate seed aerosols had no impact on SOA formation from the photo-oxidation of m-xylene and 1,3,5-trimethylbenzene.*" has been changed to "However, Cocker III et al. (2001) observed that the presence of ammonium sulfate seed aerosols had no impact on SOA formation from the photo-oxidation of m-xylene and 1,3,5-trimethylbenzene. Li et al. (2015) also suggested that no measurable differences were observed in SOA formation from m-xylene between non-seeded and seeded experiments. In this study, comparable SOA PFs for experiments with and without seed aerosols indicated wall loss of organic vapors did not significantly impact SOA production from gasoline vehicle exhaust."

**Q2**- I am still of the opinion that Figure 9 is not terribly informative nor is it easy to interpret. The individual data points are fairly noisy. Perhaps the information would be better converted in a bar graph, or merely noted in the text.

Reply: Figure 9 is an important evidence for the presence of acid-catalyzed reactions. The noisy of data points may be due to the relatively low density of the fragments m/z 88. Two smooth solid lines, based on the average values of every five data points, were added into the revised Figure 9 to highlight the higher intensity of m/z 88 for the experiment with the addition of $SO_2$.

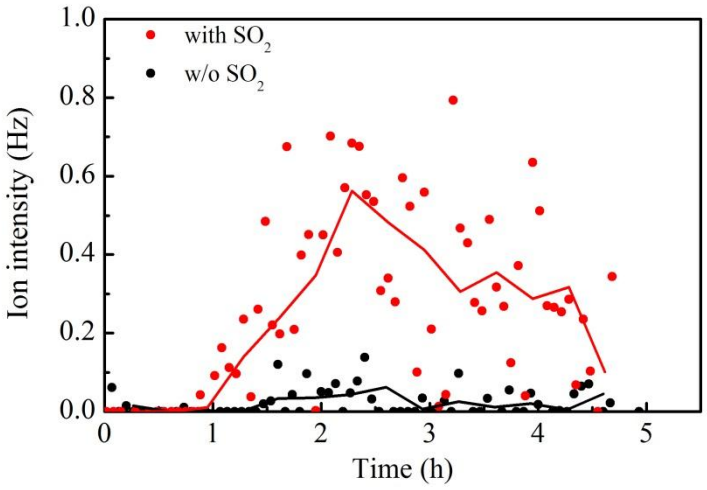


**Q3-** Likewise, I am still of the opinion that Figure 10 does not add much additional information beyond what is shown in Figure 8.

Reply: Figure 8 mainly shows the correlation between aerosol acidity and the SOA production factor, while Figure 10 provides information about the correlation between aerosol acidity and SOA formation rate.

**Q4-** I should note that the previous two comments are more style and presentation preferences than issues with scientific rigor or the overall value of the manuscript.

Reply: Addressed in Q3 and Q4.

**Q5-** The Table 5 caption seems to be incorrect.

Reply: The caption of Table 5 has been revised as follows:

"Table 5. Rate constants of sCIs used in the model."

**Q6-** Figure 1 in reviewer responses, which shows toluene decay with time and the piecewise fits to determine [OH], should go into supplemental material.

Reply: This figure has been included in supplemental material. The relevant text is also changed in the revised manuscript.

**Q7-** The authors could discuss organic nitrates a little more. It is interesting that there is so much more organic nitrate when $SO_2$ is present.

Reply: This manuscript is mainly focused on sulfate and SOA formation. Nitrates formation will be discussed in detail in a subsequent paper.

# A list of relevant changes

**Line 68-73**–Add "Multiple studies have shown that modeled SOA can only explain a fraction of the measured SOA from gasoline vehicle exhaust (Platt et al., 2013; Tkacik et al., 2014). Platt et al. (2013) found that predicted SOA accounted for approximately 20% of the SOA formed from Euro 5 gasoline vehicle exhaust. Hence, more studies are needed to bridge the gap between modeled and measured SOA from gasoline vehicle exhaust." after "…with model years prior to 1995."

**Line 208**–Add "(Figure. S1 in the Supplement)" after "were also estimated"

**Line 400**–Add "formed through acid-catalyzed heterogeneous reactions" after "a glyoxal oligomer"

**Line 402-406**–Change "However, the experiment…" to "The low intensities of m/z 88 may not indicate that oligomers formed from glyoxal are not important. It is more likely that these fragments are thermally unstable at the vaporization temperature of HR-TOF-AMS (600 ℃) and readily decompose to monomer or *gem*-diol forms before passing into the ionization region. The experiment…"

**Line 416-430** –Delete "The addition of $SO_2$ may vary the vapor wall loss rate and influence the estimation of SOA production. The wall accommodation coefficient ($\alpha_{w,i}$), governing the extent of wall deposition of a compound i, was observed to be inversely dependent on its effective saturation concentration $C_i^*$ (X. Zhang et al., 2015). Partitioning coefficients for different $C_i^*$ ranging from 0.01 to $10^6$ μg $m^{-3}$ were calculated using gas-particle partitioning theory (Donahue et al., 2006) (Table 6). Partitioning coefficients for experiments with and without the addition of $SO_2$ mainly exhibited big differences for $C_i^*$ bins of 10 and 100 μg $m^{-3}$ with $\alpha_{w,i}$ calculated to be $3.1\times10^{-7}$ and $2.0\times10^{-7}$, respectively. The wall loss rate for $C_i^*$ bin of 10 μg $m^{-3}$ would then be approximately 50% higher than that for $C_i^*$ bin of 100 μg $m^{-3}$ assuming a linear relation between wall loss rate and $\alpha_{w,i}$ (X. Zhang et al., 2015). An increase of 50% in wall loss rate would lead to 11.5% higher vapor loss to walls when assuming the wall loss rate to be $2.0\times10^{-5}$ $s^{-1}$, similar to a product of the photo-oxidation of toluene. Thus, biases of vapor wall loss rates due to the addition of $SO_2$ may have negligible influence on estimation of SOA production."

**Line 433-443**–Change "However, comparable SOA PFs for experiments with and without seed aerosols observed in this study indicated the negligible impact of seed aerosols on SOA production. Cocker III et al. (2001) also observed that the presence of ammonium sulfate seed aerosols had no impact on SOA formation from the photo-oxidation of m-xylene and 1,3,5-trimethylbenzene." to "However, Cocker III et al. (2001) observed that the presence of ammonium sulfate seed aerosols had no impact on SOA formation from the photo-oxidation of m-xylene and 1,3,5-trimethylbenzene. Li et al. (2015) also suggested that no measurable differences

were observed in SOA formation from m-xylene between non-seeded and seeded experiments. In this study, comparable SOA PFs for experiments with and without seed aerosols indicated wall loss of organic vapors did not significantly impact SOA production from gasoline vehicle exhaust."

**Line 570**–Delete the reference "Donahue, N. M., Robinson, A. L., Stanier, C. O., and Pandis, S. N.: Coupled Partitioning, Dilution, and Chemical Aging of Semivolatile Organics, Environ. Sci. Technol., 40, 2635-2643, doi:10.1021/es052297c, 2006."

**Line 662**–Add the reference "Li, L., Tang, P., and Cocker Iii, D. R.: Instantaneous nitric oxide effect on secondary organic aerosol formation from m-xylene photooxidation, Atmos. Environ., 119, 144-155, doi:10.1016/j.atmosenv.2015.08.010, 2015."

**Line 755**–Add the reference "Tkacik, D. S., Lambe, A. T., Jathar, S., Li, X., Presto, A. A., Zhao, Y. L., Blake, D., Meinardi, S., Jayne, J. T., Croteau, P. L., and Robinson, A. L.: Secondary Organic Aerosol Formation from in-Use Motor Vehicle Emissions Using a Potential Aerosol Mass Reactor, Environ. Sci. Technol., 48, 11235-11242, doi:10.1021/es502239v, 2014."

**Caption of Table 5 was revised.**

**Table 5.** Rate constants of sCIs used in the model.

**Table 6 was removed.**

**Fig. 9 was revised**.

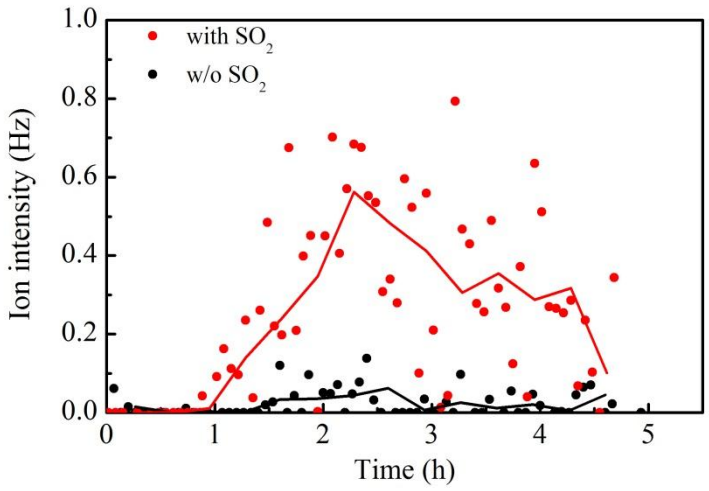


**Fig. 9.** Time evolution of m/z 88 during the aging of LDGV exhaust from vehicle III. Solid lines are derived from the average values of every five data points.

# Formation of secondary aerosols from gasoline vehicle exhaust when mixing with $SO_2$

Tengyu Liu[1,2], Xinming Wang[1]*, Qihou Hu[1], Wei Deng[1,2], Yanli Zhang[1], Xiang Ding[1], Xiaoxin Fu[1,2], Fran ̧ois Bernard[1,3], Zhou Zhang[1,2], Sujun L ̈[1,2], Quanfu He[1,2], Xinhui Bi[1], Jianmin Chen[4], Yele Sun[5], Jianzhen Yu[6], Pingan, Peng[1], Guoying Sheng[1], Jiamo Fu[1]

1. State Key Laboratory of Organic Geochemistry, Guangzhou Institute of Geochemistry, Chinese Academy of Sciences, Guangzhou 510640, China.
2. University of Chinese Academy of Sciences, Beijing 100049, China.
3. Chemical Sciences Division, NOAA Earth System Research Laboratory, Boulder, Colorado 80305, USA.
4. Shanghai Key Laboratory of Atmospheric Particle Pollution and Prevention, Department of Environmental Science & Engineering, Fudan University, Shanghai 200433, China.
5. Institute of Atmospheric Physics, Chinese Academy of Sciences, Beijing 100029, China.
6. Division of Environment, Hong Kong University of Science & Technology, Clear Water Bay, Kowloon, Hong Kong, China.

*Corresponding author:

Dr. Xinming Wang

State Key Laboratory of Organic Geochemistry

Guangzhou Institute of Geochemistry, Chinese Academy of Sciences

23 Tel: +86-20-85290180; Fax: +86-20-85290706

24 Email: wangxm@gig.ac.cn

25

## Abstract

Sulfur dioxide ($SO_2$) can enhance the formation of secondary aerosols from biogenic volatile organic compounds (VOCs), but its influence on secondary aerosol formation from anthropogenic VOCs, particularly complex mixtures like vehicle exhaust, remains uncertain. Gasoline vehicle exhaust (GVE) and $SO_2$, a typical pollutant from coal burning, are directly co-introduced into a smog chamber, in this study, to investigate the formation of secondary organic aerosols (SOA) and sulfate aerosols through photooxidation. New particle formation was enhanced while substantial sulfate was formed through the oxidation of $SO_2$ in the presence of high concentration of $SO_2$. Homogenous oxidation by OH radicals contributed a negligible fraction to the conversion of $SO_2$ to sulfate, and instead the oxidation by stabilized Criegee intermediates (sCIs), formed from alkenes in the exhaust reacting with ozone, dominated the conversion of $SO_2$. After 5 h of photochemical aging, GVE's SOA production factor revealed an increase by 60–200% in the presence of high concentration of $SO_2$. The increase could principally be attributed to acid-catalyzed SOA formation as evidenced by the strong positive linear correlation ($R^2$ = 0.97) between the SOA production factor and in-situ particle acidity calculated by AIM-II model. A high-resolution time-of-flight aerosol mass spectrometer (HR-TOF-AMS) resolved OA's relatively lower oxygen-to-carbon (O:C) (0.44±0.02) and higher hydrogen-to-carbon (H:C) (1.40±0.03) molar ratios for the GVE/$SO_2$ mixture, with a significantly lower estimated average carbon oxidation state ($OS_c$) of -0.51±0.06 than -0.19±0.08 for GVE alone. The relative higher mass loading of OA in the experiments

48 with $SO_2$ might be a significant explanation for the lower SOA oxidation degree.

## 1. Introduction

Sulfate and organic aerosols (OA) can lead to serious and complex air pollution (Parrish and Zhu, 2009) as the main components of fine particles or $PM_{2.5}$, conveying negative effects on human health (Nel, 2005). Sulfate and OA additionally affect radiative forcing on a global scale (Andreae et al., 2005; Shindell et al., 2009). Thus, a detailed understanding of the magnitude and formation pathways of sulfate and OA is critical to formulate control strategies and to accurately estimate their impact on air quality and climate. Complications often arise due to missing or underestimated oxidation pathways of sulfur dioxide ($SO_2$) (Berglen et al., 2004), the precursor of sulfate, and the unclear formation mechanisms of secondary organic aerosols (SOA) (de Gouw et al., 2005; Heald et al., 2005; Johnson et al., 2006; Volkamer et al., 2006), accounting for a large fraction of OA (Zhang et al., 2007).

Recent smog chamber studies have demonstrated that the amount of SOA formed from dilute gasoline vehicle exhaust often exceeds primary OA (POA) (Nordin et al., 2013; Platt et al., 2013; Gordon et al., 2014; Liu et al., 2015). Aromatic hydrocarbons were found to be vital SOA precursors in gasoline vehicle exhaust. Up to 90% of SOA from idling Euro 1–4 vehicle exhaust could be attributed to aromatics (Nordin et al., 2013; Liu et al., 2015). Gordon et al. (2014) concluded that traditional precursors could fully explain the SOA production from old vehicles with model years prior to 1995. Multiple studies have shown that modeled SOA can only explain a fraction of the measured SOA from gasoline vehicle exhaust (Platt et al., 2013; Tkacik et al., 2014). Platt et al. (2013) found that predicted SOA accounted for approximately 20%

of the SOA formed from Euro 5 gasoline vehicle exhaust. Hence, more studies are needed to bridge the gap between modeled and measured SOA from gasoline vehicle exhaust. Emitted primarily from coal-fired power plants and coal-burning boilers, $SO_2$, when mixed with gasoline vehicle exhaust containing the precursors for secondary nitrates and organic aerosols, $NO_x$ and aromatics, may react, complicating the formation of sulfate and SOA. Alkenes present in gasoline vehicle exhaust can react with ozone to form stabilized Criegee intermediates (sCIs), recently considered to significantly oxidize $SO_2$ and influence sulfate formation (Mauldin et al., 2012; Welz et al., 2012). On the other hand, recent smog chamber simulations indicated that $SO_2$ could enhance SOA formation from typical biogenic precursors, such as monoterpenes and isoprene through acid-catalyzed reactions (Edney et al., 2005; Kleindienst et al., 2006; Jaoui et al., 2008), but the influence of acid-catalyzed reactions on SOA formation from aromatics still remains debatable (Cao and Jang, 2007; Ng et al., 2007). Combinations of several pure chemicals, additionally, are not fully representative of $SO_2$ mixing with vehicle exhaust containing thousands of gaseous and particle-phase components (Gordon et al., 2014) in the formation of secondary aerosols under real atmospheric conditions. Till present no reports are available about the influence of $SO_2$ on secondary aerosol formation from complex vehicle exhaust.

Here we directly introduced pipe exhaust from light-duty gasoline vehicles (LDGV) and $SO_2$ into a smog chamber with a 30 $m^3$ Teflon reactor (Wang et al., 2014), to study the production of secondary aerosols: the influence of LDGV exhaust

on $SO_2$ oxidation to form sulfate aerosols and reciprocally that of $SO_2$ on SOA formation from primary organics in LDGV exhaust.

## 2. Materials and methods

### 2.1 Vehicles and fuel

In Europe, vehicle emissions are classified by "Euro Standards", currently ranging from Euro 1 to Euro 6. China implemented the Euro 1, Euro 2, Euro 3 and Euro 4 emission standards in 2000, 2004, 2007 and 2012 for LDGVs and the Euro 5 standard will be implemented in 2018. Three LDGVs were utilized in this study, one Euro 1 and two Euro 4 vehicles. They are all port fuel injected vehicles with model years ranging from 2002 to 2011. Further vehicle details are listed in Table 1. All vehicles were fueled with Grade 93# gasoline, which complies with the Euro III gasoline fuel standard. Details of the gasoline composition can be found elsewhere (Zhang et al., 2013).

### 2.2 Smog chamber experiments

Six photochemical experiments with LDGV exhaust were conducted in a 30 $m^3$ indoor smog chamber at Guangzhou Institute of Geochemistry, Chinese Academy of Sciences (GIG-CAS). Details of the smog chamber were described by Wang et al. (2014). Briefly, black lamps (1.2m-long, 60W Philips/10R BL, Royal Dutch Philips Electronics Ltd, The Netherlands) are used as a light source, providing a $NO_2$ photolysis rate of 0.49 $min^{-1}$. Two Teflon-coated fans are installed inside the reactor to guarantee thorough mixing of the introduced gas species and particles within 120 seconds. Temperature and relative humidity in the reactor were controlled at

115 approximately 25 ℃ and 50%, respectively. A schematic of the experiment setup is
116 presented in Fig. 1. Eight thermocouples are placed between the enclosure and the
117 reactor walls to control the temperature. The temperature inside the reactor (T9) was
118 measured by Siemens QFM2160 (Siemens AG, Germany).Vehicles were first
119 operated on-road to warm up the three-way catalysts for a minimal half an hour prior
120 to introducing the vehicle exhaust. Idling vehicle exhaust was then introduced directly
121 by two oil-free pumps (Gast Manufacturing, Inc, USA) into the reactor at a flow rate
122 of 40 L $min^{-1}$. Losses of volatile organic compounds (VOCs) and particles in the
123 transfer lines were estimated to be less than 5% (Liu et al., 2015). Prior to each
124 experiment, the chamber was evacuated and filled with purified dry air for at least 5
125 times, then the reactor was flushed with purified dry air for a minimal 48 h until no
126 residual hydrocarbons, $O_3$, $NO_x$, or particles were detected in the reactor. The exhaust
127 in the reactor was diluted by a factor of 13–94 compared to the tailpipe.

128 $SO_2$ was injected by a gas-tight syringe following introduction of exhaust to
129 create a mixing ratio of $SO_2$ in the reactor of approximately 150 ppb during three
130 experiments with the three vehicles. Experiments without additional $SO_2$ were also
131 conducted for each vehicle to compare and additional NO was added to adjust the
132 VOC/$NO_x$ ratios (ppb/ppb) to between 4.9 and 10.8 (Table 2). VOC/$NO_x$ ratios in
133 experiments with the same vehicle were similar with initial concentrations of $NO_x$
134 ranging from 300.8 to 458.5 ppb. After more than half an hour of primary
135 characterization, the exhaust was exposed to black light continuously for 5 h. The
136 formed SOA was characterized for another 2 to 3 h after the black lamps were

switched off to correct the particles wall loss. OH precursor and seed particles were not introduced in this study.

An array of instruments was used to characterize gas and particle phase compounds in the reactor. Gas phase $NO_x$, $O_3$ and $SO_2$ were measured with dedicated monitors (EC9810, 9841T, Ecotech, Australia, and Thermo Scientific Model 43iTLE, USA). The detection limit and accuracy of the $SO_2$ instrument are 0.2 ppb and ±1 %, respectively. Methane and CO concentrations were determined using a gas chromatography (Agilent 6980GC, USA) with a flame ionization detector and a packed column (5A Molecular Sieve 60/80 mesh, 3 m × 1/8 inch) (Zhang et al., 2012). $CO_2$ was analyzed with a HP 4890D gas chromatography (Yi et al., 2007). Gas phase organic species were measured with a Mode 7100 preconcentrator (Entech Instruments Inc., USA) coupled with an Agilent 5973N gas chromatography-mass selective detector/flame ionization detector/electron capture detector (GC-MSD/FID, Agilent Technologies, USA) (Wang and Wu, 2008, Zhang et al., 2010, 2012, 2013) and a commercial proton-transfer-reaction time-of-flight mass spectrometer (PTR-TOF-MS, Model 2000, Ionicon Analytik GmbH, Austria) (Lindinger et al., 1998; Jordan et al., 2009). $C_2$-$C_3$ and $C_4$-$C_{12}$ hydrocarbons were measured by GC-FID and GC-MSD, respectively. PTR-TOF-MS was used to determine the time-resolved concentrations of VOCs such as aromatics. The decay curve of toluene was used to derive the average hydroxyl radical (OH) concentration during each experiment.

Particle number concentrations and size distributions were measured with a scanning mobility particle sizer (SMPS, TSI Incorporated, USA, classifier model

159 3080, CPC model 3775). An aerosol density of 1.4 g $cm^{-3}$ was assumed to convert the
160 particle volume concentration into the mass concentration (Zhang et al., 2005). A
161 high-resolution time-of-flight aerosol mass spectrometer (HR-TOF-MS, Aerodyne
162 Research Incorporated, USA) was used to measure the particle chemical compositions
163 and nonrefractory PM mass (Jayne et al., 2000; DeCarlo et al., 2006). The instrument
164 was operated in the high sensitivity V-mode and high resolution W-mode alternatively
165 every two minutes. The toolkit Squirrel 1.51H was used to obtain time series of
166 various mass components (sulfate, nitrate, ammonium and organics). We used the
167 toolkit Pika 1.1H to determine the average element ratios of organics, including H:C,
168 O:C, and N:C (Aiken et al., 2007, 2008). The contribution of gas-phase $CO_2$ to the
169 m/z 44 signal was corrected with measured $CO_2$ concentrations. The HR-TOF-MS
170 was calibrated using 300 nm monodisperse ammonium nitrate particles.

171 A summary of initial experimental conditions and final results is presented in
172 Table 2 and Table 3, respectively. Total wall-loss corrected OA varied from 17.8 to
173 91.4 μg $m^{-3}$, which spans the typical urban PM concentrations in heavy polluted
174 megacities with poor air quality. POA concentrations of the experiments ranged from
175 0.13 to 0.31 μg $m^{-3}$ and are negligible compared with the formed SOA. Initial mixing
176 ratios of non-methane hydrocarbons (NMHCs) in the reactor were between 2.2 and
177 4.3 ppm, much higher than typical urban conditions. The average OH concentrations
178 during photo-oxidation ranged from 0.73 to $1.29\times10^{6}$ molecules $cm^{-3}$, approximately
179 5 times lower than that during summer daytime (Seinfeld and Pandis, 1998). Initial
180 concentrations of the reactants were maintained as similar as possible for the same

vehicle, though initial NMHCs, $NO_x$ and average OH concentrations are different from typical urban conditions, so all changes in SOA mass could be attributed to the effects of $SO_2$.

### 2.3 SOA production factors

SOA production factor (PF) (mg $kg^{-1}$) is calculated on a fuel basis:

$$PF = 10^6 \cdot [SOA] \cdot \left(\frac{[\Delta CO_2]}{MW_{CO_2}} + \frac{[\Delta CO]}{MW_{CO}} + \frac{[\Delta HC]}{MW_{HC}}\right)^{-1} \cdot \frac{\omega_C}{MW_C} \qquad (1)$$

where $[\Delta CO_2]$, $[\Delta CO]$, and $[\Delta HC]$ are the background corrected concentrations of $CO_2$, CO and the total hydrocarbons in the reactor in μg $m^{-3}$; [SOA] is the concentration of wall-loss corrected SOA in μg $m^{-3}$; $MW_{CO2}$, $MW_{CO}$, $MW_{HC}$, and $MW_C$ are the molecular weights of $CO_2$, CO, HC and C. $\omega_C$ (0.85) is the carbon intensity of the gasoline (Kirchstetter et al., 1999). Total hydrocarbons measured in this study include methane and $C_2$-$C_{12}$ hydrocarbons. The carbon content of each hydrocarbon was respectively calculated and then summed in Eq. (1).

### 2.4 Determination of OH concentration

Decay of toluene measured by PTR-TOF-MS is used to determine the average OH concentration during each experiment. Changes in the toluene concentration over time can be expressed as:

$$\frac{d[toluene]}{dt} = -k \cdot [OH] \cdot [toluene] \qquad (2)$$

where $k$ is the rate constant for the reaction between toluene and OH radical. The value of $k$ is obtained from the Master Chemical Mechanism version 3.3 or MCM v3.3 (http://www.chem.leeds.ac.uk/MCM) (Jenkin et al., 2003). Assuming a constant OH concentration during an experiment, we can integrate Eq. (2) to get Eq. (3):

$$\ln\left(\frac{[toluene]_0}{[toluene]_t}\right) = k \cdot [OH] \cdot t \qquad (3)$$

So by plotting $ln([\text{toluene}]_0/[\text{toluene}]_t)$ versus time t, we can obtain a slope that equals $k \times [OH]$. The average OH concentration is then calculated as:

$$[OH] = \frac{slope}{k} \qquad (4)$$

Average OH concentrations were determined when the black lamps were on. Segmented OH concentrations were also estimated (Figure. S1 in the Supplement) and listed in Table S1 ~~in the Supplement~~ for experiments with the addition of $SO_2$. Similar concentrations of sCIs were determined in subsequent section 2.5 when average and segmented OH concentrations were respectively used for the same experiment.

**2.5 Determination of the steady state concentration of sCIs**

Ozonolysis of alkenes will form a primary ozonide through a 1,3-cycloaddition of ozone across the olefinic bond. The primary ozonide then rapidly decomposes to two carbonyl compounds, called excited CIs, which can be stabilized by collision to form sCIs (Heard et al., 2004; Johnson and Marston, 2008).

$$\text{alkene} + O_3 \longrightarrow \phi\text{sCIs} + \text{products} \qquad (R1)$$

where $\phi$ represents the yield of sCIs from ozonolysis of alkenes. The four main losses of sCIs are reactions with $H_2O$, $SO_2$ and $NO_2$ and unimolecular decomposition.

$$\text{sCIs} + H_2O \longrightarrow \text{products} \qquad (R2)$$

$$\text{sCIs} + SO_2 \longrightarrow SO_3 + \text{products} \qquad (R3)$$

$$\text{sCIs} + NO_2 \longrightarrow \text{products} \qquad (R4)$$

$$\text{sCIs} \longrightarrow \text{products} \qquad (R5)$$

The steady state concentration of sCIs will be

$$sCIs_{steady\ state} = \frac{\phi K_{R1}[O_3][alkene]}{K_{R2}[H_2O] + K_{R3}[SO_2] + K_{R4}[NO_2] + K_{R5}} \quad (5)$$

where $K_{R1}$ is the rate coefficient for the ozonolysis of alkene; $K_{R2}$, $K_{R3}$, $K_{R4}$ and $K_{R5}$ represent the rate constant for reactions of sCIs with $H_2O$, $SO_2$, $NO_2$ and decomposition, respectively. This equation was widely used to predict the steady state concentration of sCIs in the atmosphere (Welz et al., 2012; Newland et al., 2015).

The steady state concentration of sCIs throughout the entire experiment was estimated in this study. The production rate of sCIs was dependent on both the concentrations and composition of alkenes in the exhaust. Detailed gas-phase mechanisms of alkenes from the MCM v3.3 were run to determine the time-resolved concentrations of sCIs in the experiments. The concentrations of alkenes included in the model and the category of sCIs are presented in Table 4. N-alkenes and branched alkenes respectively contributed 89.9%-93.0% and 7.0%-10.1% of the alkenes, with ethene and propene as two main components accounting for 66.8%-81.3%. Only the gas-phase mechanisms of alkenes were included in the model, with the concentrations of OH radicals, $SO_2$, $O_3$ and $NO_2$ constrained to measured concentrations. Thus, the neglect of alkanes and aromatics would not influence the steady state concentrations of sCIs, as was confirmed by running the models including alkanes and aromatics. $K_{R2}$, $K_{R3}$, $K_{R4}$ and $K_{R5}$ for $CH_2OO$, $CH_3CHOO$, and $(CH_3)_2COO$ used in the model were listed in Table 5. The rate coefficients for other sCIs including $C_2H_5CHOO$, $C_3H_7CHOO$, $C_2H_5(CH_3)COO$ and $(CH_3)_2CHCHOO$ reacted with $H_2O$, $SO_2$, $NO_2$ and their unimolecular decomposition were assumed to be same as $CH_2OO$. This

assumption seems reasonable as the precursors of $C_2H_5CHOO$, $C_3H_7CHOO$, $C_2H_5(CH_3)COO$ and $(CH_3)_2CHCHOO$ contributed only a small portion of alkenes in this study. The yields of $CH_2OO$, $CH_3CHOO$, and $(CH_3)_2COO$ used in the model were 0.37, 0.38 and 0.28, respectively, while yields of other sCIs were assumed to be same as $CH_2OO$.

**2.6 Wall loss corrections**

The loss of particles and organic vapors onto the reactor walls must be accounted for to accurately quantify the SOA production. A detailed discussion of these corrections can be found elsewhere (Liu et al., 2015). The loss of particles onto the walls was treated as a first-order process (McMurry and Grosjean, 1985). The wall-loss rate constant was determined separately for each experiment by fitting the SMPS and AMS data with first-order kinetics when UV lamps were switched off. By applying this rate to the entire experiment, we use the same method as Pathak et al. (2007) to correct the wall loss of the particles. The wall loss of particles is a size-dependent process, therefore, the presence of nucleation would influence wall loss correction of the particles due to the rapid loss of nucleation mode particles. As shown in a previous study, particle wall loss rates could not be accurately quantified for the particles generated in the nucleation event (Keywood et al., 2004). The impact of the nucleation event on wall-loss estimate is considered to be negligible as less than 5% of the particle mass is in the nucleation mode twenty minutes after nucleation for all experiments in this study.

Wall deposition of organic vapors can lead to the underestimation of SOA

production (Matsunaga and Ziemann, 2010; X. Zhang et al., 2014, 2015). Wall deposition of a compound has recently been established as related with its volatility (Zhang et al., 2015). The extent that wall deposition of organic vapors impacts on SOA production depends on the competition of organic vapors depositing onto walls and suspended particles. Here, we assumed that gas-particle partitioning of organic vapors dominated their wall depositions and thus organic vapors were considered to only partition onto suspended particles.

As the collection efficiency of sulfate in the HR-TOF-AMS can vary due to the coating of OA onto sulfate, we used AMS data combined with SMPS data to derive the time-resolved concentrations of OA, sulfate, ammonium and nitrate. The emission of black carbon (BC) from LDGVs was negligible according to a previous study (Liu et al., 2015), thus the ratio of OA to inorganic aerosols from the AMS was used to split the total particle mass measured by SMPS into the mass of OA, sulfate, ammonium and nitrate (Gordon et al., 2014; Liu et al., 2015).

# 3. Results and discussion

## 3.1 Formation of sulfate

Fig. 2 shows the temporal evolution of gas– and particle–phase species during the photochemical aging of emissions from vehicle III with and without adding $SO_2$. NO was injected to adjust the VOC/$NO_x$ ratio at approximately time = -0.25 h for both experiments. After the black lamps were switched on, NO was rapidly consumed in less than 1 h. Mass concentrations of secondary aerosols rapidly ascended following photooxidation with or without $SO_2$ for approximately 1 h, stabilizing after

approximately 4 h of photo-oxidation (Figs. 2, 3, and 4). Substantial sulfate was formed synchronously with OA for experiments with $SO_2$ with the maximum particle number concentrations at 5.4–48 times of those without $SO_2$ (Table 1, Fig. 5), indicating enhanced new particle formation (NPF) when adding $SO_2$. As the precursor of sulfuric acid ($H_2SO_4$), $SO_2$ at higher concentrations would lead to additional formation of $H_2SO_4$, thereby increasing the nucleation rates and total particle number concentrations (Sipila et al., 2010). The S-bearing organic fragments $C_xH_yO_zS$ determined by HR-TOF-AMS can be used as marker ions to quantify organosulfates (Huang et al., 2015). In this study the fragments $C_xH_yO_zS$ were almost not appreciable. Using the methods of Huang et al. (2015), we estimated the mass ratio of organosulfates to sulfate was less than 0.5%. Thus the formation of organosulfates could be negligible in this study.

Substantial nitrates were formed for vehicles I and II (Figs. 3a and 4a) and could be attributed to ammonium or organic nitrates. The identification of ammonium and organic nitrates may be obtained from the $NO^+/NO_2^+$ ratio, which is typically substantially higher for organic nitrates compared with ammonium nitrate (Farmer et al., 2010; Sato et al., 2010). The $NO^+/NO_2^+$ ratios for experiments I-2 and II-2 were 1.99-2.60, within the range 1.08-2.81 for ammonium nitrate (Farmer et al., 2010; Sato et al., 2010), suggesting that nitrates detected in the two experiments could be attributed to ammonium nitrate. Ammonium nitrate was likely formed by reactions of nitric acid formed from $NO_x$ oxidation and ammonia, which is substantially higher in China's LDGV exhaust (Liu et al., 2014). The $NO^+/NO_2^+$ ratios for experiments with

313 $SO_2$ were 3.9-5.0, significantly higher than ratios measured for ammonium nitrate and
314 also similar to ratios for organic nitrates (3.82-5.84) from the photo-oxidation of
315 aromatic hydrocarbons (Sato et al., 2010), indicating organic nitrates dominated
316 nitrate formation in these experiments. High concentration of $SO_2$ suppressed the
317 formation of ammonium nitrate in experiments with $SO_2$ as $NH_3$ was liable to react
318 with sulfuric acid rather than nitric acid (Pathak et al., 2009).

319 Formation rates of sulfate, derived from the differential of concentration-time
320 plots of sulfate, exhibited burst increases at the initial stage of sulfate formation and
321 then decreased to near zero 5 h after sulfate formation initiated (Fig. 6a). The
322 maximum formation rate of sulfate in experiments I–2, II–2 and III–2 was 61.5, 21.6
323 and 113 μg $m^{-3}$ $h^{-1}$, respectively, extremely higher than the rate of 0.17–0.37 ppbv $h^{-1}$
324 (0.73–1.59 μg $m^{-3}$ $h^{-1}$ under NTP condition) through gas-phase oxidation of $SO_2$
325 during the daytime in the Pearl River Delta (PRD) region of China in the summer of
326 2006 (Xiao et al., 2009), and also more than ten times higher than the maximum
327 sulfate formation rate of 4.79 μg $m^{-3}$ $h^{-1}$ observed at an urban site in Beijing during
328 the Beijing Olympic Games in 2008 (Zhang et al., 2011). The formation rate of sulfate
329 was related to the concentrations of $SO_2$ and OH, which were respectively
330 approximately 7 times higher and 2-16 times lower than those in the study of Xiao et
331 al. (2009). Significant differences of sulfate formation rates between chamber and
332 ambient observations could, however, indicate that there might be other processes
333 dominating the oxidation of $SO_2$ rather than gas-phase oxidation by OH in this study.

334 $SO_2$ was typically deemed to be oxidized by OH radicals through homogeneous

reactions in gas-phase (Calvert et al., 1978), or by $H_2O_2$ and $O_3$ through in-cloud processes in aqueous-phase (Lelieveld and Heintzenberg, 1992) that, however, could be negligible in this study due to RH of approximate 50%. As shown in Fig. 7, the loss rate of $SO_2$ through homogeneous reactions with OH radicals in the three experiments ranged from 0.0023 to 0.0034 $h^{-1}$, accounting for only 2.4%–4.6% of the total loss rate of $SO_2$. The initial concentrations of alkenes in the experiments with $SO_2$ varied from 248 to 547 ppb, contributing 7.7%–23.5% of the total NMHCs. The high content of alkenes in the exhaust might form a mass of sCIs through the reaction with ozone. Recent studies indicated the rate coefficient of $CH_2OO$ with $SO_2$ was 50 to 10000 times larger than that used in tropospheric models (Welz et al., 2012). The oxidation of $SO_2$ by sCIs may be as significant as that by OH radicals in the atmosphere. The oxidation rate of $SO_2$ for experiments I-2 and III-2, through the reactions with sCIs, was calculated to be $0.065 \pm 0.029$ $h^{-1}$ and $0.042 \pm 0.020$ $h^{-1}$ (Fig. 7), respectively, accounting for 66.9% and 61.4% of the total loss rate of $SO_2$. Considering the variability of sCIs throughout the entire experiment, we concluded that sCIs were virtually responsible for the oxidation of $SO_2$ in experiments I-2 and III-2. The oxidation rate of $SO_2$ through the reactions with sCIs for the experiment II-2 was estimated to be $0.028 \pm 0.015$ $h^{-1}$, contributing 31.5% of the total loss rate of $SO_2$. The unexplained loss of $SO_2$ might be a result of heterogeneous oxidation in the presence of LDGV exhaust containing massive aerosols and gaseous species. He et al. (2014) found that $SO_2$ could react with $NO_2$ on the surface of mineral dust to promote the conversion of $SO_2$ to sulfate. As shown in Fig. 5, the initial particle number for

vehicle II was approximately 5000 $cm^{-3}$, nearly 40-50 times higher than those for vehicle I and III, providing larger aerosol surface areas for the oxidation of $SO_2$ by $NO_2$. However, quantification of $SO_2$ oxidation by $NO_2$ on the surface of existing aerosols is difficult due to the lack of reaction rate constant (He et al., 2014). We speculate that the reaction between $SO_2$ and $NO_2$ on the surface of existing aerosols might explain the difference between the total loss rate of $SO_2$ and the sum of sCIs and OH oxidation for vehicle II.

### 3.2 SOA production

Fuel-based SOA production factors (PF), expressed as SOA production in milligram (mg) after 5 h photooxidation of LDGV exhaust emitted when per kilogram (kg) gasoline was burned, all increased substantially when adding $SO_2$, 60%–200% above that without $SO_2$ (Fig. 8a), although the selected cars' emission standards varied from Euro-I to Euro-IV. The in-situ particle acidities at the time when SOA formation rate peaks were calculated as $H^+$ concentrations based on AIM-II model $H^+$–$NH_4^+$–$SO_4^{2-}$–$NO_3^-$–$H_2O$ with gas-aerosol partitioning disabled (http://www.aim.env.uea.ac.uk/aim/model2/model2a.php) (Clegg et al., 1998; Wexler and Clegg, 2002). Inputs to the model include temperature, RH, [$SO_4^{2-}$], [$NO_3^-$], [$NH_4^+$] and $[H^+]_{total}$, calculated based on ion balance. $SO_4^{2-}$, $NH_4^+$ and $NO_3^-$ contributed virtually all of the aerosol phase ions mass in this study, thus determining the aerosol acidity. Though other ions (i.e., $Ca^{2+}$, $Mg^{2+}$, $K^+$ and $Na^+$) had negligible influence on the aerosol acidity, it is worth noting that the reported values of $H^+$ may be the upper bound. The in-situ particle acidities with the addition of $SO_2$ were 1.6–

379 3.7 times as high as those without the addition of $SO_2$ (Table 3). This elevated particle
380 acidity could largely explain the higher PFs of SOA from LDGV exhaust with $SO_2$,
381 supported by the strong positive linear correlations ($R^2$ = 0.965, $P$<0.01) between
382 SOA PFs and the in-situ particle acidities (Fig. 8b). Aromatic hydrocarbons are vital
383 SOA precursors in gasoline vehicle exhaust (Nordin et al., 2013; Gordon et al., 2014;
384 Liu et al., 2015). The influence of particle acidity on SOA formation from aromatics
385 is still debatable. Cao and Jang (2007) found that the presence of acid seeds with [$H^+$]
386 concentrations of 240-860 nmol $m^{-3}$ significantly increased the SOA yields from
387 oxidation of toluene and 1,3,5-trimethylbenzene compared with yields using neutral
388 seed aerosols. However, Ng et al. (2007) observed no influence of particle acidity on
389 SOA yields from the aromatics possibly due to the low content of aerosol water. SOA
390 production from gasoline vehicle exhaust was enhanced in this study, even at a low
391 level of [$H^+$] concentrations ranging from 7.4 to 27.1 nmol $m^{-3}$. Gas-phase oxidation
392 products of aromatic hydrocarbons in the exhaust, like multifunctional carbonyl
393 glyoxal, would be transformed more rapidly to low volatility products through
394 acid-catalyzed heterogeneous reactions (Jang et al., 2002; Cao and Jang, 2007) and
395 thus caused increasing SOA production. Aerosol water is needed for the hydration of
396 carbonyls and therefore it influences the acid-catalyzed reactions. Liquid water
397 content (LWC) in this study was not measured but predicted by the AIM-II model,
398 with an average value of 5.5±4.5 μg $m^{-3}$ when SOA formation rate peaks, ensuring
399 the occurrence of acid-catalyzed reactions. Fig. 9 shows the ion intensity of fragment
400 m/z 88 that can arise only from a glyoxal oligomer formed through acid-catalyzed

heterogeneous reactions (Liggio et al., 2015). The scatter of the data might be due to the low intensity of m/z 88. The low intensities of m/z 88 may not indicate that oligomers formed from glyoxal are not important. It is more likely that these fragments are thermally unstable at the vaporization temperature of HR-TOF-AMS (600 ℃) and readily decompose to monomer or *gem*-diol forms before passing into the ionization region. ~~However, t~~The experiment with the addition of $SO_2$, with higher particle acidity, exhibited relatively higher m/z 88 intensity. This indicated the important role of acid-catalyzed heterogeneous reactions in SOA formation from gasoline vehicle exhaust. A photo-oxidation experiment of exhaust from vehicle I in the presence of ammonium sulfate seeds (53.3 μg $m^{-3}$) with RH of 59% (Table 2) was conducted to explore the effect of sulfate on SOA formation as particle acidity is typically driven by sulfate. The SOA production factor was 22.2 mg $kg^{-1}$ fuel, comparable with 26.2 mg $kg^{-1}$ fuel for experiment I-1, indicating that sulfate may not directly influence SOA production. Thus, the SOA production was indeed dependent on the particle acidity.

~~The addition of $SO_2$ may vary the vapor wall loss rate and influence the estimation of SOA production. The wall accommodation coefficient ($\alpha_{w,i}$), governing the extent of wall deposition of a compound i, was observed to be inversely dependent on its effective saturation concentration $C_i^*$ (X. Zhang et al., 2015). Partitioning coefficients for different $C_i^*$ ranging from 0.01 to $10^6$ μg $m^{-3}$ were calculated using gas-particle partitioning theory (Donahue et al., 2006) (Table 6). Partitioning coefficients for experiments with and without the addition of $SO_2$ mainly exhibited~~

~~big differences for $C_i^*$ bins of 10 and 100 μg $m^{-3}$ with $\alpha_{w,i}$ calculated to be $3.1\times10^{-7}$ and $2.0\times10^{-7}$, respectively. The wall loss rate for $C_i^*$ bin of 10 μg $m^{-3}$ would then be approximately 50% higher than that for $C_i^*$ bin of 100 μg $m^{-3}$ assuming a linear relation between wall loss rate and $\alpha_{w,i}$ (X. Zhang et al., 2015). An increase of 50% in wall loss rate would lead to 11.5% higher vapor loss to walls when assuming the wall loss rate to be $2.0\times10^{-5}$ $s^{-1}$, similar to a product of the photo-oxidation of toluene. Thus, biases of vapor wall loss rates due to the addition of $SO_2$ may have negligible influence on estimation of SOA production.~~ Recent studies indicated that the presence of high concentrations of seed aerosols might decrease the loss of organic vapors to the walls and thus increase the SOA formation (Kroll et al., 2007; X. Zhang et al., 2014, 2015). However, Cocker III et al. (2001) ~~also~~ observed that the presence of ammonium sulfate seed aerosols had no impact on SOA formation from the photo-oxidation of m-xylene and 1,3,5-trimethylbenzene~~–~~. Li et al. (2015) also suggested that no measurable differences were observed in SOA formation from m-xylene between non-seeded and seeded experiments. In this study, comparable SOA PFs for experiments with and without seed aerosols ~~observed in this study~~ indicated wall loss of organic vapors did not significantly impact SOA production from gasoline vehicle exhaust~~the negligible impact of seed aerosols on SOA production~~. ~~Cocker III et al. (2001) also observed that the presence of ammonium sulfate seed aerosols had no impact on SOA formation from the photo-oxidation of m-xylene and 1,3,5-trimethylbenzene.~~

SOA formation rates, derived from the differential of concentration-time plots of

SOA, exhibited similar trends as sulfate with a burst increase at the initial stage of SOA formation (Fig. 6b). The average SOA formation rates for vehicles I, II and III with $SO_2$ were 1.1, 1.2 and 4.4 times as high as those without $SO_2$, respectively, although the maximum rate for vehicle II with $SO_2$ was lower. Here we particularly focused on the burst increase stage of SOA and sulfate, which may be related to fast increase of $PM_{2.5}$ and occurrence of haze (He et al., 2014). Fig. 10 shows the correlation between SOA formation rate and particle acidity. Plotted data corresponded to data selected from Fig. 6 when SOA formation rate was higher than zero to when the rate reached the maximum value. Significant linear correlations ($P<0.05$, $R^2>0.88$) between SOA formation rate and particle acidity during this stage for experiments with $SO_2$ suggest that acid-catalyzed heterogeneous reactions might play an important role in the rapid formation of SOA (Jang et al., 2002). The fitted slopes for vehicle I, II and III were 3.96, 0.82 and 3.14, respectively, suggesting other factors, including alkene abundance, may influence the SOA formation rate. The initial concentration of alkenes for experiments I-2, II-2 and III-2 was 547 ppb, 248 ppb and 353 ppb, respectively, consistent with the variation of the slopes. Higher alkene content would increase the formation rate of sCIs, which could rapidly oxidize $SO_2$ to sulfuric acid, thus influence the aerosol acidity.

### 3.3 Oxidation state

After 5 h of photo-oxidation, SOA's molar ratios of oxygen-to-carbon (O:C) and hydrogen-to-carbon (H:C) resolved by HR-TOF-AMS, were plotted on a Van Krevelen diagram (Heald et al., 2010) in Fig. 11. Concentrations of POA were lower

than 0.5 μg $m^{-3}$, typically regarded as not appreciable (Presto et al., 2014) and insufficient to determine the initial H:C and O:C, thus only SOA data were plotted on the diagram. Relatively lower O:C (0.44±0.02) and higher H:C (1.40±0.03) for the mixture of $SO_2$ and exhaust were observed than those for exhaust alone. The oxidation state of carbon ($OS_c$), estimated from O:C and H:C, can be used to describe the chemistry and oxidative evolution of atmospheric organic aerosols (Kroll et al., 2011). Further calculated $OS_c$ revealed an average lower level of -0.51±0.06 for SOA formed from LDGV exhaust with $SO_2$ when compared to that of -0.19±0.08 without $SO_2$, with all within or near the $OS_c$ range of -0.5–0 for semi-volatile OOA (SV-OOA) (Aiken et al., 2008). The relatively lower $OS_c$ with $SO_2$ indicated a lower oxidation degree of SOA. A difference in H:C and O:C for m-xylene SOA with neutral and acidic seed particles was not observed by Loza et al. (2012), thus acid-catalyzed heterogeneous reactions may not influence the oxidation degree of SOA in this study. Shilling et al. (2009) observed a lower O:C of SOA formed from the dark ozonolysis of α-pinene at a higher mass loading of organic aerosols and suggested that compounds partitioning into the particle phase at lower loadings were more oxygenated. Kang et al. (2011) also observed that the oxidation degree of OA decreased rapidly as the OA mass concentration increased for the same amount of OH exposure. Given that the average OH concentrations were similar for the same vehicle (Table 2), the relative higher mass loading of OA in the experiments with $SO_2$ may lead to the lower O:C and thus decrease the oxidation degree of OA. The O:C ratios were observed to decrease 0.1 with an increase of approximately 50 μg $m^{-3}$ of OA

concentrations for m-xylene and p-xylene (Kang et al., 2011). However, in this study the slope was 0.1 ΔO:C for approximately 26 μg $m^{-3}$ ΔOA. The differences may be due to that some other precursors other than aromatics contributed to SOA formation from gasoline vehicle exhaust (Liu et al., 2015).

The slope of -0.87 (Fig. 11) for the mixture of $SO_2$ and exhaust, slightly higher than those for exhaust alone (Liu et al., 2015), indicates that SOA formation in these experiments is a combination of carboxylic acid and alcohol/peroxide formation (Heald et al., 2010; Ng et al., 2011). The slope of -0.87 and intercept of approximately 1.8 are similar to the observation for ambient data with a slope of approximately -1 and intercept approximately 1.8 (Heald et al., 2010), suggesting that SOA chemistry for the mixture of $SO_2$ and gasoline vehicle exhaust is atmospheric relevant.

## 4. Conclusions

A series of chamber experiments investigating the formation of secondary aerosols from the mixture of $SO_2$ and gasoline vehicle exhaust were conducted. The high content of alkenes in gasoline vehicle exhaust formed numerous sCIs, dominating the formation of sulfate while elevated particle acidity, resulting from the formation of sulfuric acid, enhanced SOA production from the gasoline vehicle exhaust. We concluded that $SO_2$ and gasoline vehicle exhaust can enhance each other in forming secondary aerosols. High concentration of $SO_2$ and high levels of aerosol acidity combined with rapid increase of LDGVs in heavily polluted cities such as Beijing (Pathak et al., 2009; He et al., 2014) might consequently worsen the air quality in the absence of stricter control strategies on emissions of $SO_2$ and vehicle exhaust.

Previous studies indicated that high content of alkenes in China's gasoline oil was damaging for the control of ozone in ambient air (Y. Zhang et al., 2013, 2015). Our results suggested that the incomplete combustion of gasoline with high content of alkenes might also induce the formation of sCIs, facilitating the production of secondary aerosols. The limit of alkenes content in China was lowered to 24% by volume in the newly established Level V gasoline fuel standard from 28% by volume in the Level IV gasoline fuel standard. This limit remains substantially higher when compared to those in USA or in Europe, and in particular, 6 times that in California, USA. Thus, limiting the content of alkenes in China's gasoline might benefit the control of both ozone and secondary aerosols.

**Acknowledgments**

This study was supported by Strategic Priority Research Program of the Chinese Academy of Sciences (Grant No. XDB05010200), the Ministry of Science and Technology of China (Project No. 2012IM030700), National Natural Science Foundation of China (Project No. 41025012/41121063) and Guangzhou Institute of Geochemistry (GIGCAS 135 project Y234161001).

## References


Aiken, A. C., DeCarlo, P. F., and Jimenez, J. L.: Elemental Analysis of Organic Species with Electron Ionization High-Resolution Mass Spectrometry, Analy. Chem., 79, 8350-8358, doi:10.1021/ac071150w, 2007.

Aiken, A. C., DeCarlo, P. F., Kroll, J. H., Worsnop, D. R., Huffman, J. A., Docherty, K. S., Ulbrich, I. M., Mohr, C., Kimmel, J. R., Sueper, D., Sun, Y., Zhang, Q., Trimborn, A., Northway, M., Ziemann, P. J., Canagaratna, M. R., Onasch, T. B., Alfarra, M. R., Prevot, A. S. H., Dommen, J., Duplissy, J., Metzger, A., Baltensperger, U., and Jimenez, J. L.: O/C and OM/OC Ratios of Primary, Secondary, and Ambient Organic Aerosols with High-Resolution Time-of-Flight Aerosol Mass Spectrometry, Environ. Sci. Technol., 42, 4478-4485, doi:10.1021/es703009q, 2008.

Andreae, M. O., Jones, C. D., and Cox, P. M.: Strong present-day aerosol cooling implies a hot future, Nature, 435, 1187-1190, 2005.

Berglen, T. F., Berntsen, T. K., Isaksen, I. S. A., and Sundet, J. K.: A global model of the coupled sulfur/oxidant chemistry in the troposphere: The sulfur cycle, J. Geophys. Res.-Atmos., 109, D19310, doi:10.1029/2003JD003948, 2004.

Calvert, J. G., Su, F., Bottenheim, J. W., and Strausz, O. P.: Mechanism of the homogeneous oxidation of sulfur dioxide in the troposphere, Atmos. Environ., 12, 197-226, doi:10.1016/0004-6981(78)90201-9, 1978.

Cao, G., and Jang, M.: Effects of particle acidity and UV light on secondary organic aerosol formation from oxidation of aromatics in the absence of $NO_x$, Atmos.

552 Environ., 41, 7603-7613, doi:10.1016/j.atmosenv.2007.05.034, 2007.
553 Clegg, S. L., Brimblecombe, P., and Wexler, A. S.: Thermodynamic Model of the
554 System $H^+$–$NH_4^+$–$SO_4^{2-}$–$NO_3^-$–$H_2O$ at Tropospheric Temperatures, J. Phys. Chem.
555 A, 102, 2137-2154, doi:10.1021/jp973042r, 1998.
556 Cocker III, D. R., Mader, B. T., Kalberer, M., Flagan, R. C., and Seinfeld, J. H.: The
557 effect of water on gas–particle partitioning of secondary organic aerosol: II.
558 m-xylene and 1,3,5-trimethylbenzene photooxidation systems, Atmos. Environ., 35,
559 6073-6085, doi:10.1016/S1352-2310(01)00405-8, 2001.
560 de Gouw, J. A., Middlebrook, A. M., Warneke, C., Goldan, P. D., Kuster, W. C.,
561 Roberts, J. M., Fehsenfeld, F. C., Worsnop, D. R., Canagaratna, M. R., Pszenny, A.
562 A. P., Keene, W. C., Marchewka, M., Bertman, S. B., and Bates, T. S.: Budget of
563 organic carbon in a polluted atmosphere: Results from the New England Air
564 Quality Study in 2002, J. Geophys. Res.-Atmos., 110, D16305,
565 doi:10.1029/2004JD005623, 2005.
566 DeCarlo, P. F., Kimmel, J. R., Trimborn, A., Northway, M. J., Jayne, J. T., Aiken, A.
567 C., Gonin, M., Fuhrer, K., Horvath, T., Docherty, K. S., Worsnop, D. R., and
568 Jimenez, J. L.: Field-Deployable, High-Resolution, Time-of-Flight Aerosol Mass
569 Spectrometer, Anal. Chem., 78, 8281-8289, doi:10.1021/ac061249n, 2006.
570 ~~Donahue, N. M., Robinson, A. L., Stanier, C. O., and Pandis, S. N.: Coupled~~
571 ~~Partitioning, Dilution, and Chemical Aging of Semivolatile Organics, Environ. Sci.~~
572 ~~Technol., 40, 2635-2643, doi:10.1021/es052297c, 2006.~~
573 Edney, E. O., Kleindienst, T. E., Jaoui, M., Lewandowski, M., Offenberg, J. H., Wang,

574 W., and Claeys, M.: Formation of 2-methyl tetrols and 2-methylglyceric acid in
575 secondary organic aerosol from laboratory irradiated isoprene/$NO_x$/$SO_2$/air
576 mixtures and their detection in ambient $PM_{2.5}$ samples collected in the eastern
577 United States, Atmos. Environ., 39, 5281-5289,
578 doi:10.1016/j.atmosenv.2005.05.031, 2005.
579 Farmer, D. K., Matsunaga, A., Docherty, K. S., Surratt, J. D., Seinfeld, J. H., Ziemann,
580 P. J., and Jimenez, J. L.: Response of an aerosol mass spectrometer to
581 organonitrates and organosulfates and implications for atmospheric chemistry, P.
582 Natl. Acad. Sci., 107, 6670-6675, doi:10.1073/pnas.0912340107, 2010.
583 Fenske, J. D., Hasson, A. S., Ho, A. W., and Paulson, S. E.: Measurement of Absolute
584 Unimolecular and Bimolecular Rate Constants for $CH_3CHOO$ Generated by the
585 trans-2-Butene Reaction with Ozone in the Gas Phase, J. Phys. Chem. A, 104,
586 9921-9932, doi:10.1021/jp0016636, 2000.
587 Gordon, T. D., Presto, A. A., May, A. A., Nguyen, N. T., Lipsky, E. M., Donahue, N.
588 M., Gutierrez, A., Zhang, M., Maddox, C., Rieger, P., Chattopadhyay, S.,
589 Maldonado, H., Maricq, M. M., and Robinson, A. L.: Secondary organic aerosol
590 formation exceeds primary particulate matter emissions for light-duty gasoline
591 vehicles, Atmos. Chem. Phys., 14, 4661-4678, doi:10.5194/acp-14-4661-2014,
592 2014.
593 He, H., Wang, Y., Ma, Q., Ma, J., Chu, B., Ji, D., Tang, G., Liu, C., Zhang, H., and
594 Hao, J.: Mineral dust and $NO_x$ promote the conversion of $SO_2$ to sulfate in heavy
595 pollution days, Sci. Rep., 4, 4172, doi:10.1038/srep04172, 2014.

596 Heald, C. L., Jacob, D. J., Park, R. J., Russell, L. M., Huebert, B. J., Seinfeld, J. H.,
597 Liao, H., and Weber, R. J.: A large organic aerosol source in the free troposphere
598 missing from current models, Geophys. Res. Lett., 32, L18809,
599 do:10.1029/2005GL023831, 2005.
600 Heald, C. L., Kroll, J. H., Jimenez, J. L., Docherty, K. S., DeCarlo, P. F., Aiken, A. C.,
601 Chen, Q., Martin, S. T., Farmer, D. K., and Artaxo, P.: A simplified description of
602 the evolution of organic aerosol composition in the atmosphere, Geophys. Res.
603 Lett., 37, L08803, doi:10.1029/2010gl042737, 2010.
604 Heard, D. E., Carpenter, L. J., Creasey, D. J., Hopkins, J. R., Lee, J. D., Lewis, A. C.,
605 Pilling, M. J., Seakins, P. W., Carslaw, N., and Emmerson, K. M.: High levels of the
606 hydroxyl radical in the winter urban troposphere, Geophys. Res. Lett., 31, L18112,
607 doi:10.1029/2004GL020544, 2004.
608 Huang, D. D., Li, Y. J., Lee, B. P., and Chan, C. K.: Analysis of Organic Sulfur
609 Compounds in Atmospheric Aerosols at the HKUST Supersite in Hong Kong Using
610 HR-ToF-AMS, Environ. Sci. Technol., 49, 3672-3679, doi:10.1021/es5056269,
611 2015.
612 Jang, M., Czoschke, N. M., Lee, S., and Kamens, R. M.: Heterogeneous Atmospheric
613 Aerosol Production by Acid-Catalyzed Particle-Phase Reactions, Science, 298,
614 814-817, doi:10.1126/science.1075798, 2002.
615 Jaoui, M., Edney, E. O., Kleindienst, T. E., Lewandowski, M., Offenberg, J. H.,
616 Surratt, J. D., and Seinfeld, J. H.: Formation of secondary organic aerosol from
617 irradiated α-pinene/toluene/$NO_x$ mixtures and the effect of isoprene and sulfur

618 dioxide, J. Geophys. Res. -Atmos., 113, D09303, doi:10.1029/2007JD009426,
619 2008.
620 Jayne, J. T., Leard, D. C., Zhang, X., Davidovits, P., Smith, K. A., Kolb, C. E., and
621 Worsnop, D. R.: Development of an Aerosol Mass Spectrometer for Size and
622 Composition Analysis of Submicron Particles, Aerosol. Sci. Tech., 33, 49-70,
623 doi:10.1080/027868200410840, 2000.
624 Jenkin, M. E., Saunders, S. M., Wagner, V., and Pilling, M. J.: Protocol for the
625 development of the Master Chemical Mechanism, MCM v3 (Part B): tropospheric
626 degradation of aromatic volatile organic compounds, Atmos. Chem. Phys., 3,
627 181-193, doi:10.5194/acp-3-181-2003, 2003.
628 Johnson, D., Utembe, S. R., Jenkin, M. E., Derwent, R. G., Hayman, G. D., Alfarra,
629 M. R., Coe, H., and McFiggans, G.: Simulating regional scale secondary organic
630 aerosol formation during the TORCH 2003 campaign in the southern UK, Atmos.
631 Chem. Phys., 6, 403-418, doi:10.5194/acp-6-403-2006, 2006.
632 Jordan, A., Haidacher, S., Hanel, G., Hartungen, E., Mark, L., Seehauser, H.,
633 Schottkowsky, R., Sulzer, P., and Mark, T. D.: A high resolution and high sensitivity
634 proton-transfer-reaction time-of-flight mass spectrometer (PTR-TOF-MS), Int. J.
635 Mass. Spectrom., 286, 122-128, 2009.
636 Kang, E., Toohey, D. W., and Brune, W. H.: Dependence of SOA oxidation on organic
637 aerosol mass concentration and OH exposure: experimental PAM chamber studies,
638 Atmos. Chem. Phys., 11, 1837-1852, doi:10.5194/acp-11-1837-2011, 2011.
639 Keywood, M. D., Varutbangkul, V., Bahreini, R., Flagan, R. C., and Seinfeld, J. H.:

640 Secondary Organic Aerosol Formation from the Ozonolysis of Cycloalkenes and
641 Related Compounds, Environ. Sci. Technol., 38, 4157-4164,
642 doi:10.1021/es035363o, 2004.
643 Kirchstetter, T. W., Harley, R. A., Kreisberg, N. M., Stolzenburg, M. R., and Hering, S.
644 V.: On-road measurement of fine particle and nitrogen oxide emissions from light-
645 and heavy-duty motor vehicles, Atmos. Environ., 33, 2955-2968,
646 doi:10.1016/S1352-2310(99)00089-8, 1999.
647 Kleindienst, T. E., Edney, E. O., Lewandowski, M., Offenberg, J. H., and Jaoui, M.:
648 Secondary Organic Carbon and Aerosol Yields from the Irradiations of Isoprene
649 and α-Pinene in the Presence of $NO_x$ and $SO_2$, Environ. Sci. Technol., 40,
650 3807-3812, doi:10.1021/es052446r, 2006.
651 Kroll, J. H., Chan, A. W. H., Ng, N. L., Flagan, R. C., and Seinfeld, J. H.: Reactions
652 of Semivolatile Organics and Their Effects on Secondary Organic Aerosol
653 Formation, Environ. Sci. Technol., 41, 3545-3550, doi:10.1021/es062059x, 2007.
654 Kroll, J. H., Donahue, N. M., Jimenez, J. L., Kessler, S. H., Canagaratna, M. R.,
655 Wilson, K. R., Altieri, K. E., Mazzoleni, L. R., Wozniak, A. S., Bluhm, H., Mysak,
656 E. R., Smith, J. D., Kolb, C. E., and Worsnop, D. R.: Carbon oxidation state as a
657 metric for describing the chemistry of atmospheric organic aerosol, Nat. Chem., 3,
658 133-139, doi:10.1038/nchem.948, 2011.
659 Lelieveld, J., and Heintzenberg, J.: Sulfate Cooling Effect on Climate Through
660 In-Cloud Oxidation of Anthropogenic $SO_2$, Science, 258, 117-120,
661 doi:10.1126/science.258.5079.117, 1992.

662 Li, L., Tang, P., and Cocker Iii, D. R.: Instantaneous nitric oxide effect on secondary
663 organic aerosol formation from m-xylene photooxidation, Atmos. Environ., 119,
664 144-155, doi:10.1016/j.atmosenv.2015.08.010, 2015.
665 Liggio, J., Li, S.-M., and McLaren, R.: Heterogeneous Reactions of Glyoxal on
666 Particulate Matter: Identification of Acetals and Sulfate Esters, Environ. Sci.
667 Technol., 39, 1532-1541, doi:10.1021/es048375y, 2005.
668 Lindinger, W., Hansel, A., and Jordan, A.: On-line monitoring of volatile organic
669 compounds at pptv levels by means of proton-transfer-reaction mass spectrometry
670 (PTR-MS) medical applications, food control and environmental research, Int. J.
671 Mass Spectrometry., 173, 191-241, doi:10.1016/S0168-1176(97)00281-4, 1998.
672 Liu, T. Y., Wang, X. M., Wang, B. G., Ding, X., Deng, W., Lü, S. J., and Zhang, Y. L.:
673 Emission factor of ammonia ($NH_3$) from on-road vehicles in China: tunnel tests in
674 urban Guangzhou, Environ. Res. Lett., 9, 064027,
675 doi:10.1088/1748-9326/9/6/064027, 2014.
676 Liu, T., Wang, X., Deng, W., Hu, Q., Ding, X., Zhang, Y., He, Q., Zhang, Z., Lü, S.,
677 Bi, X., Chen, J., and Yu, J.: Secondary organic aerosol formation from
678 photochemical aging of light-duty gasoline vehicle exhausts in a smog chamber,
679 Atmos. Chem. Phys., 15, 9049-9062, doi:10.5194/acp-15-9049-2015, 2015.
680 Loza, C. L., Chhabra, P. S., Yee, L. D., Craven, J. S., Flagan, R. C., and Seinfeld, J. H.:
681 Chemical aging of m-xylene secondary organic aerosol: laboratory chamber study,
682 Atmos. Chem. Phys., 12, 151-167, doi:10.5194/acp-12-151-2012, 2012.
683 Matsunaga, A., and Ziemann, P. J.: Gas-Wall Partitioning of Organic Compounds in a

684 Teflon Film Chamber and Potential Effects on Reaction Product and Aerosol Yield
685 Measurements, Aerosol Sci. Tech., 44, 881-892,
686 doi:10.1080/02786826.2010.501044, 2010.
687 Mauldin Iii, R. L., Berndt, T., Sipila, M., Paasonen, P., Petaja, T., Kim, S., Kurten, T.,
688 Stratmann, F., Kerminen, V. M., and Kulmala, M.: A new atmospherically relevant
689 oxidant of sulphur dioxide, Nature, 488, 193-196, doi:10.1038/nature11278, 2012.
690 McMurry, P. H., and Grosjean, D.: Gas and aerosol wall losses in Teflon film smog
691 chambers, Environ. Sci. Technol., 19, 1176-1182, doi:10.1021/es00142a006, 1985.
692 Nel, A.: Air Pollution-Related Illness: Effects of Particles, Science, 308, 804-806,
693 doi:10.1126/science.1108752, 2005.
694 Newland, M. J., Rickard, A. R., Alam, M. S., Vereecken, L., Munoz, A., Rodenas, M.,
695 and Bloss, W. J.: Kinetics of stabilised Criegee intermediates derived from alkene
696 ozonolysis: reactions with $SO_2$, $H_2O$ and decomposition under boundary layer
697 conditions, Phys. Chem. Chem. Phys., 17, 4076-4088, doi:10.1039/C4CP04186K,
698 2015.
699 Ng, N. L., Kroll, J. H., Chan, A. W. H., Chhabra, P. S., Flagan, R. C., and Seinfeld, J.
700 H.: Secondary organic aerosol formation from m-xylene, toluene, and benzene,
701 Atmos. Chem. Phys., 7, 3909-3922, doi:10.5194/acp-7-3909-2007, 2007.
702 Ng, N. L., Canagaratna, M. R., Jimenez, J. L., Chhabra, P. S., Seinfeld, J. H., and
703 Worsnop, D. R.: Changes in organic aerosol composition with aging inferred from
704 aerosol mass spectra, Atmos. Chem. Phys., 11, 6465-6474,
705 doi:10.5194/acp-11-6465-2011, 2011.

706 Nordin, E. Z., Eriksson, A. C., Roldin, P., Nilsson, P. T., Carlsson, J. E., Kajos, M. K.,
707 Hellén, H., Wittbom, C., Rissler, J., Löndahl, J., Swietlicki, E., Svenningsson, B.,
708 Bohgard, M., Kulmala, M., Hallquist, M., and Pagels, J. H.: Secondary organic
709 aerosol formation from idling gasoline passenger vehicle emissions investigated in
710 a smog chamber, Atmos. Chem. Phys., 13, 6101-6116,
711 doi:10.5194/acp-13-6101-2013, 2013.
712 Ouyang, B., McLeod, M. W., Jones, R. L., and Bloss, W. J.: $NO_3$ radical production
713 from the reaction between the Criegee intermediate $CH_2OO$ and $NO_2$, Phys. Chem.
714 Chem. Phys., 15, 17070-17075, doi:10.1039/C3CP53024H, 2013.
715 Parrish, D. D., and Zhu, T.: Clean Air for Megacities, Science, 326, 674-675,
716 doi:10.1126/science.1176064, 2009.
717 Pathak, R. K., Stanier, C. O., Donahue, N. M., and Pandis, S. N.: Ozonolysis of
718 alpha-pinene at atmospherically relevant concentrations: Temperature dependence
719 of aerosol mass fractions (yields), J. Geophys. Res.-Atmos, 112, D03201,
720 doi:10.1029/2006jd007436, 2007.
721 Pathak, R. K., Wu, W. S., and Wang, T.: Summertime $PM_{2.5}$ ionic species in four
722 major cities of China: nitrate formation in an ammonia-deficient atmosphere,
723 Atmos. Chem. Phys., 9, 1711-1722, doi:10.5194/acp-9-1711-2009, 2009.
724 Platt, S. M., El Haddad, I., Zardini, A. A., Clairotte, M., Astorga, C., Wolf, R., Slowik,
725 J. G., Temime-Roussel, B., Marchand, N., Ježek, I., Drinovec, L., Močnik, G.,
726 Möhler, O., Richter, R., Barmet, P., Bianchi, F., Baltensperger, U., and Prévôt, A. S.
727 H.: Secondary organic aerosol formation from gasoline vehicle emissions in a new

mobile environmental reaction chamber, Atmos. Chem. Phys., 13, 9141-9158, doi:10.5194/acp-13-9141-2013, 2013.

Presto, A. A., Gordon, T. D., and Robinson, A. L.: Primary to secondary organic aerosol: evolution of organic emissions from mobile combustion sources, Atmos. Chem. Phys., 14, 5015-5036, doi:10.5194/acp-14-5015-2014, 2014.

Sato, K., Takami, A., Isozaki, T., Hikida, T., Shimono, A., and Imamura, T.: Mass spectrometric study of secondary organic aerosol formed from the photo-oxidation of aromatic hydrocarbons, Atmos. Environ., 44, 1080-1087, doi:10.1016/j.atmosenv.2009.12.013, 2010.

Seinfeld, J. and Pandis, S. N.: From air pollution to climate change, Atmospheric Chemistry and Physics, 2nd Edn., p. 208, 1998.

Shilling, J. E., Chen, Q., King, S. M., Rosenoern, T., Kroll, J. H., Worsnop, D. R., DeCarlo, P. F., Aiken, A. C., Sueper, D., Jimenez, J. L., and Martin, S. T.: Loading-dependent elemental composition of α-pinene SOA particles, Atmos. Chem. Phys., 9, 771-782, doi:10.5194/acp-9-771-2009, 2009.

Shindell, D. T., Faluvegi, G., Koch, D. M., Schmidt, G. A., Unger, N., and Bauer, S. E.: Improved Attribution of Climate Forcing to Emissions, Science, 326, 716-718, doi:10.1126/science.1174760, 2009.

Sipila, M., Berndt, T., Petaja, T., Brus, D., Vanhanen, J., Stratmann, F., Patokoski, J., Mauldin, R. L., Hyvarinen, A. P., Lihavainen, H., and Kulmala, M.: The Role of Sulfuric Acid in Atmospheric Nucleation, Science, 327, 1243-1246, doi:10.1126/science.1180315, 2010.

750 Taatjes, C. A., Welz, O., Eskola, A. J., Savee, J. D., Scheer, A. M., Shallcross, D. E.,
751 Rotavera, B., Lee, E. P. F., Dyke, J. M., Mok, D. K. W., Osborn, D. L., and Percival,
752 C. J.: Direct Measurements of Conformer-Dependent Reactivity of the Criegee
753 Intermediate $CH_3CHOO$, Science, 340, 177-180, doi:10.1126/science.1234689,
754 2013.
755 Tkacik, D. S., Lambe, A. T., Jathar, S., Li, X., Presto, A. A., Zhao, Y. L., Blake, D.,
756 Meinardi, S., Jayne, J. T., Croteau, P. L., and Robinson, A. L.: Secondary Organic
757 Aerosol Formation from in-Use Motor Vehicle Emissions Using a Potential Aerosol
758 Mass Reactor, Environ. Sci. Technol., 48, 11235-11242, doi:10.1021/es502239v,
759 2014.
760 Volkamer, R., Jimenez, J. L., San Martini, F., Dzepina, K., Zhang, Q., Salcedo, D.,
761 Molina, L. T., Worsnop, D. R., and Molina, M. J.: Secondary organic aerosol
762 formation from anthropogenic air pollution: Rapid and higher than expected,
763 Geophys. Res. Lett., 33, L17811, doi:10.1029/2006gl026899, 2006.
764 Wang, X., and Wu, T.: Release of Isoprene and Monoterpenes during the Aerobic
765 Decomposition of Orange Wastes from Laboratory Incubation Experiments,
766 Environ. Sci. Technol., 42, 3265-3270, doi:10.1021/es702999j, 2008.
767 Wang, X., Liu, T., Bernard, F., Ding, X., Wen, S., Zhang, Y., Zhang, Z., He, Q., Lü, S.,
768 Chen, J., Saunders, S., and Yu, J.: Design and characterization of a smog chamber
769 for studying gas-phase chemical mechanisms and aerosol formation, Atmos. Meas.
770 Tech., 7, 301-313, doi:10.5194/amt-7-301-2014, 2014.
771 Welz, O., Savee, J. D., Osborn, D. L., Vasu, S. S., Percival, C. J., Shallcross, D. E.,

772 and Taatjes, C. A.: Direct Kinetic Measurements of Criegee Intermediate ($CH_2OO$)
773 Formed by Reaction of $CH_2I$ with $O_2$, Science, 335, 204-207,
774 doi:10.1126/science.1213229, 2012.
775 Wexler, A. S. and Clegg, S. L.: Atmospheric aerosol models for systems including the
776 ions $H^+$, $NH_4^+$, $Na^+$, $SO_4^{2-}$, $NO_3^-$, $Cl^-$, $Br^-$, and $H_2O$, J. Geophys. Res., 107(D14),
777 4207, doi:10.1029/2001JD000451, 2002.
778 Xiao, R., Takegawa, N., Kondo, Y., Miyazaki, Y., Miyakawa, T., Hu, M., Shao, M.,
779 Zeng, L. M., Hofzumahaus, A., Holland, F., Lu, K., Sugimoto, N., Zhao, Y., and
780 Zhang, Y. H.: Formation of submicron sulfate and organic aerosols in the outflow
781 from the urban region of the Pearl River Delta in China, Atmos. Environ., 43,
782 3754-3763, doi:10.1016/j.atmosenv.2009.04.028, 2009.
783 Yi, Z., Wang, X., Sheng, G., Zhang, D., Zhou, G., and Fu, J.: Soil uptake of carbonyl
784 sulfide in subtropical forests with different successional stages in south China, J.
785 Geophy. Res.-Atmos., 112, D08302, doi:10.1029/2006JD008048, 2007.
786 Zhang, Q., Jimenez, J. L., Canagaratna, M. R., Allan, J. D., Coe, H., Ulbrich, I.,
787 Alfarra, M. R., Takami, A., Middlebrook, A. M., Sun, Y. L., Dzepina, K., Dunlea,
788 E., Docherty, K., DeCarlo, P. F., Salcedo, D., Onasch, T., Jayne, J. T., Miyoshi, T.,
789 Shimono, A., Hatakeyama, S., Takegawa, N., Kondo, Y., Schneider, J., Drewnick,
790 F., Borrmann, S., Weimer, S., Demerjian, K., Williams, P., Bower, K., Bahreini, R.,
791 Cottrell, L., Griffin, R. J., Rautiainen, J., Sun, J. Y., Zhang, Y. M., and Worsnop, D.
792 R.: Ubiquity and dominance of oxygenated species in organic aerosols in
793 anthropogenically-influenced Northern Hemisphere midlatitudes, Geophys. Res.

794 Lett., 34, L13801, doi:10.1029/2007gl029979, 2007.
795 Zhang, X., Cappa, C. D., Jathar, S. H., McVay, R. C., Ensberg, J. J., Kleeman, M. J.,
796 and Seinfeld, J. H.: Influence of vapor wall loss in laboratory chambers on yields of
797 secondary organic aerosol, P. Natl. Acad. Sci., 111, 5802–5807,
798 doi:10.1073/pnas.1404727111, 2014.
799 Zhang, X., Schwantes, R. H., McVay, R. C., Lignell, H., Coggon, M. M., Flagan, R.
800 C., and Seinfeld, J. H.: Vapor wall deposition in Teflon chambers, Atmos. Chem.
801 Phys., 15, 4197-4214, doi:10.5194/acp-15-4197-2015, 2015.
802 Zhang, Y., Guo, H., Wang, X., Simpson, I. J., Barletta, B., Blake, D. R., Meinardi, S.,
803 Rowland, F. S., Cheng, H., Saunders, S. M., and Lam, S. H. M.: Emission patterns
804 and spatiotemporal variations of halocarbons in the Pearl River Delta region,
805 southern China, J. Geophy. Res.-Atmos., 115, D15309, doi:10.1029/2009JD013726,
806 2010.
807 Zhang, Y., Wang, X., Blake, D. R., Li, L., Zhang, Z., Wang, S., Guo, H., Lee, F. S. C.,
808 Gao, B., Chan, L., Wu, D., and Rowland, F. S.: Aromatic hydrocarbons as ozone
809 precursors before and after outbreak of the 2008 financial crisis in the Pearl River
810 Delta region, south China, J. Geophy. Res.-Atmos., 117, D15306,
811 doi:10.1029/2011JD017356, 2012.
812 Zhang, Y., Wang, X., Zhang, Z., Lü, S., Shao, M., Lee, F. S. C., and Yu, J.: Species
813 profiles and normalized reactivity of volatile organic compounds from gasoline
814 evaporation in China, Atmos. Environ., 79, 110-118,
815 doi:10.1016/j.atmosenv.2013.06.029, 2013.

816 Zhang, Y., Wang, X., Zhang, Z., Lü, S., Huang, Z., and Li, L.: Sources of C2–C4
817 alkenes, the most important ozone nonmethane hydrocarbon precursors in the Pearl
818 River Delta region, Sci. Total Environ., 502, 236-245,
819 doi:10.1016/j.scitotenv.2014.09.024, 2015.
820 Zhang, Y. M., Zhang, X. Y., Sun, J. Y., Lin, W. L., Gong, S. L., Shen, X. J., and Yang,
821 S.: Characterization of new particle and secondary aerosol formation during
822 summertime in Beijing, China, Tellus B, 63, doi:10.3402/tellusb.v63i3.16221,
823 2011.
824

825 **Table 1.** Detailed information of the three LDGVs.

| ID | Emission standard class | Vehicle | Model year | Mileage (km) | Displacement ($cm^3$) | Power (kW) | Weight (kg) |
|---|---|---|---|---|---|---|---|
| Ⅰ | Euro4 | Golf | 2011 | 25000 | 1598 | 77 | 1295 |
| Ⅱ | Euro4 | Sunny | 2011 | 9448 | 1498 | 82 | 1069 |
| Ⅲ | Euro1 | Accord | 2002 | 237984 | 2298 | 110 | 1423 |

826

827

828

829 **Table 2.** Summary of the initial conditions during the photooxidation of LDGV
830 exhaust.

| Exp #[a] | OH ($\times10^6$ molecules $cm^{-3}$) | T (℃) | RH (%) | VOC /$NO_x$ | NMHCs (ppbv) | NO (ppbv) | $NO_2$ (ppbv) | $SO_2$ (ppbv) |
|---|---|---|---|---|---|---|---|---|
| I–1 | 0.88 | 25.0±0.8 | 52.9±2.0 | 9.3 | 2896 | 300.6 | 9.5 | 8.6 |
| I–2 | 1.19 | 25.5±0.3 | 53.6±2.5 | 7.7 | 2323 | 281.4 | 19.5 | 151.8 |
| I–3[b] | 1.45 | 23.9±0.9 | 59.0±4.1 | 7.9 | 2447 | 300.0 | 10.2 | 8.9 |
| II–1 | 1.29 | 24.6±0.5 | 52.5±1.7 | 10.8 | 4313 | 374 | 24.7 | 9 |
| II–2 | 1.08 | 24.2±0.7 | 55.9±2.5 | 9 | 3220 | 356 | 2.6 | 151.9 |
| III–1 | 0.73 | 24.1±0.6 | 57.0±2.0 | 6 | 2582 | 431 | 0.6 | 9.2 |
| III–2 | 0.79 | 24.3±0.3 | 57.9±1.2 | 4.9 | 2243 | 454.6 | 3.9 | 154.1 |

831 [a] Photooxidation experiments of LDGV exhaust named with I, II and III refers to different
832 vehicles.
833 [b] Ammonium sulfate (53.3 μg $m^{-3}$) was introduced as seed aerosols.
834

835 **Table 3.** Summary of the final results during the photooxidation of LDGV exhaust.

| Exp # | POA ($\mu g\ m^{-3}$) | SOA ($\mu g\ m^{-3}$) | Sulfate ($\mu g\ m^{-3}$) | Ammonium ($\mu g\ m^{-3}$) | Nitrate ($\mu g\ m^{-3}$) | Particle number ($cm^{-3}$)[a] | $[H^+]$[b] ($nmol\ m^{-3}$) |
|---|---|---|---|---|---|---|---|
| I–1 | 0.31 | 77.6 | 0.7 | 17.1 | 65.9 | 85182 | 12.5 |
| I–2 | 0.21 | 91.2 | 67.5 | 17.6 | 6.1 | 563705 | 21.9 |
| II–1 | 0.28 | 30.7 | - | 2.6 | 5.6 | 7427 | 10.4 |
| II–2 | 0.13 | 37.3 | 38.1 | 9.7 | 1.9 | 357673 | 16.5 |
| III–1 | 0.17 | 17.6 | - | 0.1 | 0.7 | 116143 | 7.4 |
| III–2 | 0.23 | 77 | 76.7 | 19.2 | 5.3 | 630620 | 27.1 |

836 [a] Maximum particle number concentrations were without wall loss corrections.

837 [b] The concentration of $H^+$ in particle phase shown here was the value when the SOA formation rate

838 reached the maximum during each experiment.

839

840 **Table 4.** Concentrations of alkenes included in the model and the category of sCIs.

| Sepecies | Concentration (ppb) | | | sCIs |
|---|---|---|---|---|
| | I-2 | II-2 | III-2 | |
| ethene | 333.1 | 113.8 | 202.0 | $CH_2OO$ |
| propene | 95.8 | 50.3 | 52.6 | $CH_2OO$, $CH_3CHOO$ |
| 1-butene | 30.9 | 49.1 | 13.1 | $CH_2OO$, $C_2H_5CHOO$ |
| cis-2-butene | 7.6 | 4.8 | 7.1 | $CH_3CHOO$ |
| trans-2-butene | 9.9 | 6.4 | 9.6 | $CH_3CHOO$ |
| 1-pentene | 3.8 | 0.3 | 3.1 | $CH_2OO$, $C_3H_7CHOO$ |
| cis-2-pentene | 5.2 | 1.2 | 5.2 | $CH_3CHOO$, $C_2H_5CHOO$ |
| trans-2-pentene | 8.5 | 2.6 | 9.4 | $CH_3CHOO$, $C_2H_5CHOO$ |
| 2-methyl-1-butene | 11.9 | 5.4 | 12.4 | $CH_2OO$, $C_2H_5(CH_3)COO$ |
| 3-methyl-1-butene | 2.4 | 0.8 | 2.4 | $CH_2OO$, $(CH_3)_2CHCHOO$ |
| 2-methyl-2-butene | 17.8 | 10.9 | 22.7 | $CH_3CHOO$, $(CH_3)_2COO$ |
| cis-2-hexene | 0.8 | 0 | 1.5 | $CH_3CHOO$, $C_3H_7CHOO$ |

841

842

**Table 5.** ~~Summary of the final results during the photooxidation of LDGV exhaust~~Rate constants of sCIs used in the model.

| Stabilized CIs | $10^{15}$ $K_{R2}$ ($cm^3$ $molecule^{-1}s^{-1}$) | $10^{11}$ $K_{R3}$ ($cm^3$ $molecule^{-1}s^{-1}$) | $10^{12}$ $K_{R4}$ ($cm^3$ $molecule^{-1}s^{-1}$) | $K_{R5}$ ($s^{-1}$) |
|---|---|---|---|---|
| $CH_2OO$ | 0.025[a] | 3.9[b] | 7.0[b] | 0[c] |
| $CH_3CHOO$ | 7.0[d] | 4.55[d] | 2.0[d] | 67.5[e] |
| $(CH_3)_2COO$ | 2.1[c] | 2.4[c] | 2.0[c] | 151[c] |

[a] (Ouyang et al., 2013); [b] (Welz et al., 2012); [c] (Newland et al., 2015); [d] (Taatjes et al., 2013);

[e] Average of $K_{R5}$ from Fenske et al. (2000) and Newland et al. (2015).

**Table 6.** Partitioning coefficients for different $C_i^*$ calculated using gas-particle partitioning theory.

| $\log_{10} C_i^*$ ($\mu g\ m^{-3}$) | I-1 | I-2 | II-1 | II-2 | III-1 | III-3 |
|---|---|---|---|---|---|---|
| -2 | 1.000 | 1.000 | 1.000 | 1.000 | 0.999 | 1.000 |
| -1 | 0.999 | 0.999 | 0.997 | 0.997 | 0.994 | 0.999 |
| 0 | 0.987 | 0.989 | 0.968 | 0.974 | 0.946 | 0.987 |
| 1 | 0.886 | 0.901 | 0.754 | 0.789 | 0.638 | 0.885 |
| 2 | 0.437 | 0.477 | 0.235 | 0.272 | 0.150 | 0.435 |
| 3 | 0.072 | 0.084 | 0.030 | 0.036 | 0.017 | 0.071 |
| 4 | 0.008 | 0.009 | 0.003 | 0.004 | 0.002 | 0.008 |
| 5 | 0.001 | 0.001 | 0.000 | 0.000 | 0.000 | 0.001 |
| 6 | 0.000 | 0.000 | 0.000 | 0.000 | 0.000 | 0.000 |

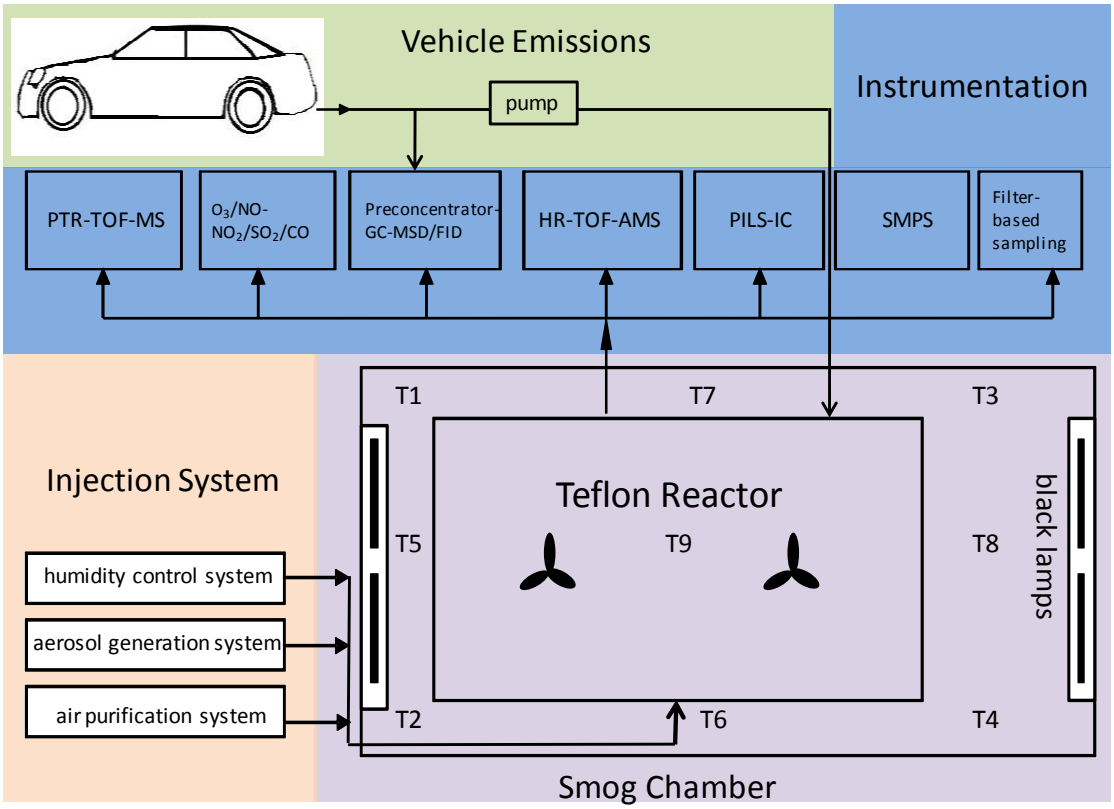


852

853 **Fig. 1.** Schematic of the GIG-CAS smog chamber facility and vehicle exhaust

854 injection system.

855

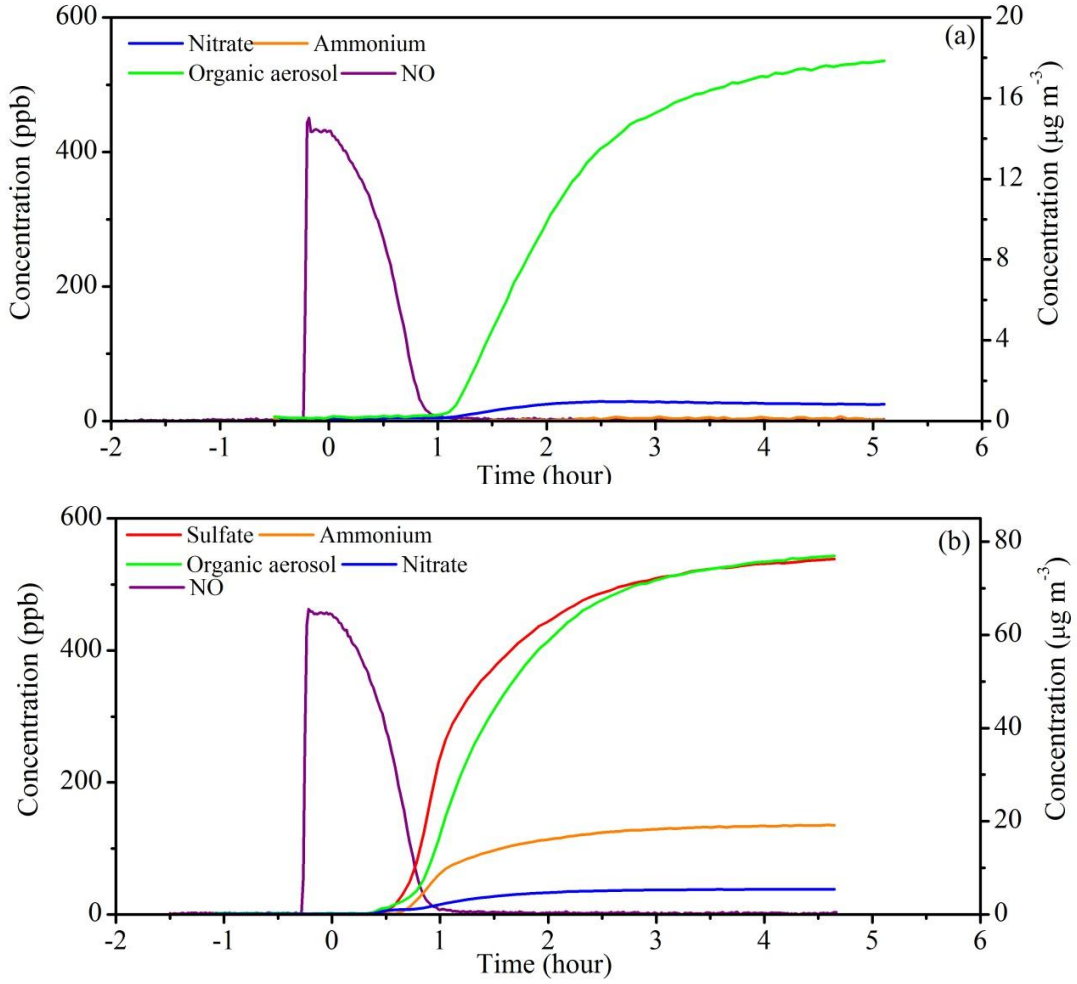


856

857 **Fig. 2.** Concentration–time plots of NO (left-y axis) and particle–phase species
858 (right-y axis) during the photochemical aging of emissions from vehicle III. (a)
859 Without $SO_2$, and (b) with $SO_2$. The concentrations of particle-phase species are
860 wall-loss corrected. At time =0 h, the black lamps were turned on.

861

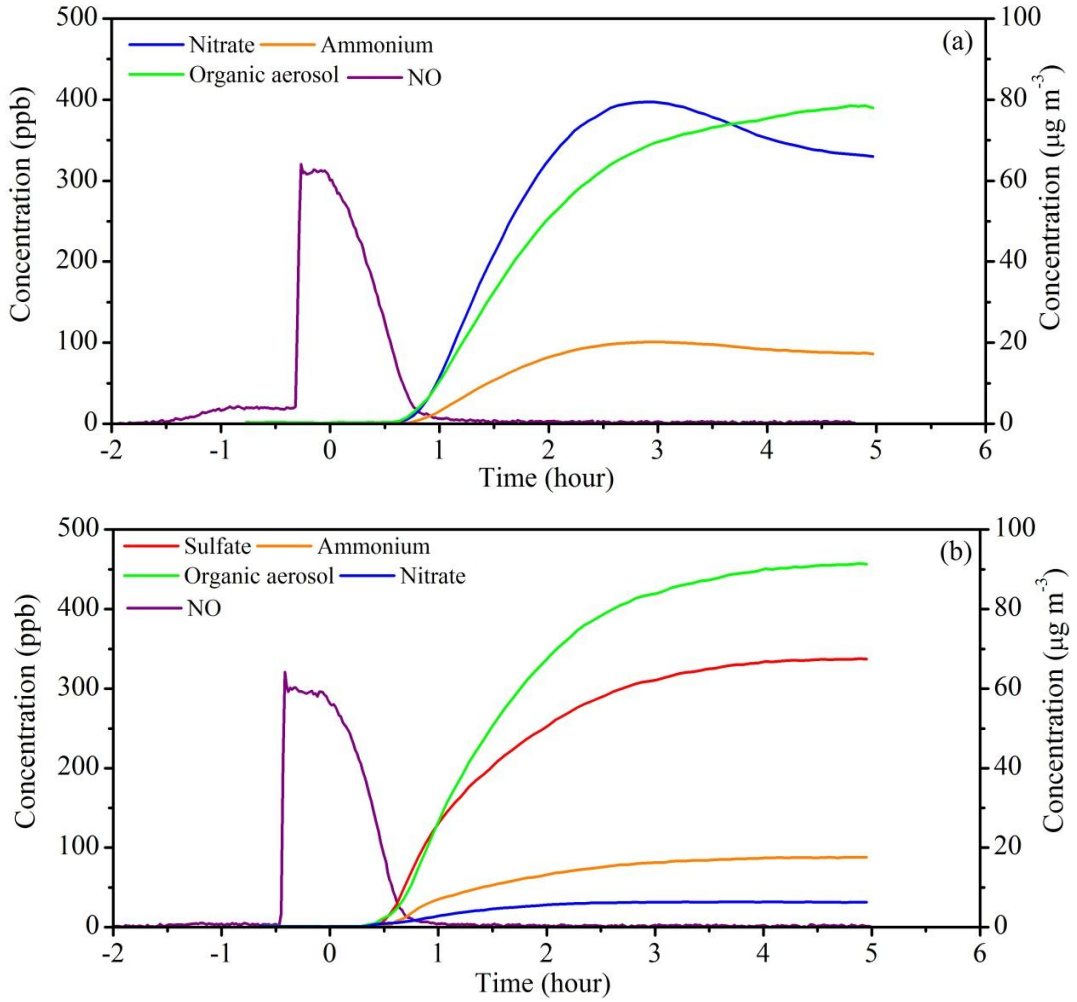


862

863 **Fig. 3.** Concentration–time plots of NO (left-y axis) and particle–phase species

864 (right-y axis) during the photochemical aging of emissions from vehicle I. (a) Without

865 $SO_2$, and (b) with $SO_2$. The concentrations of particle-phase species are wall-loss

866 corrected. At time =0 h, the black lamps were turned on.

867

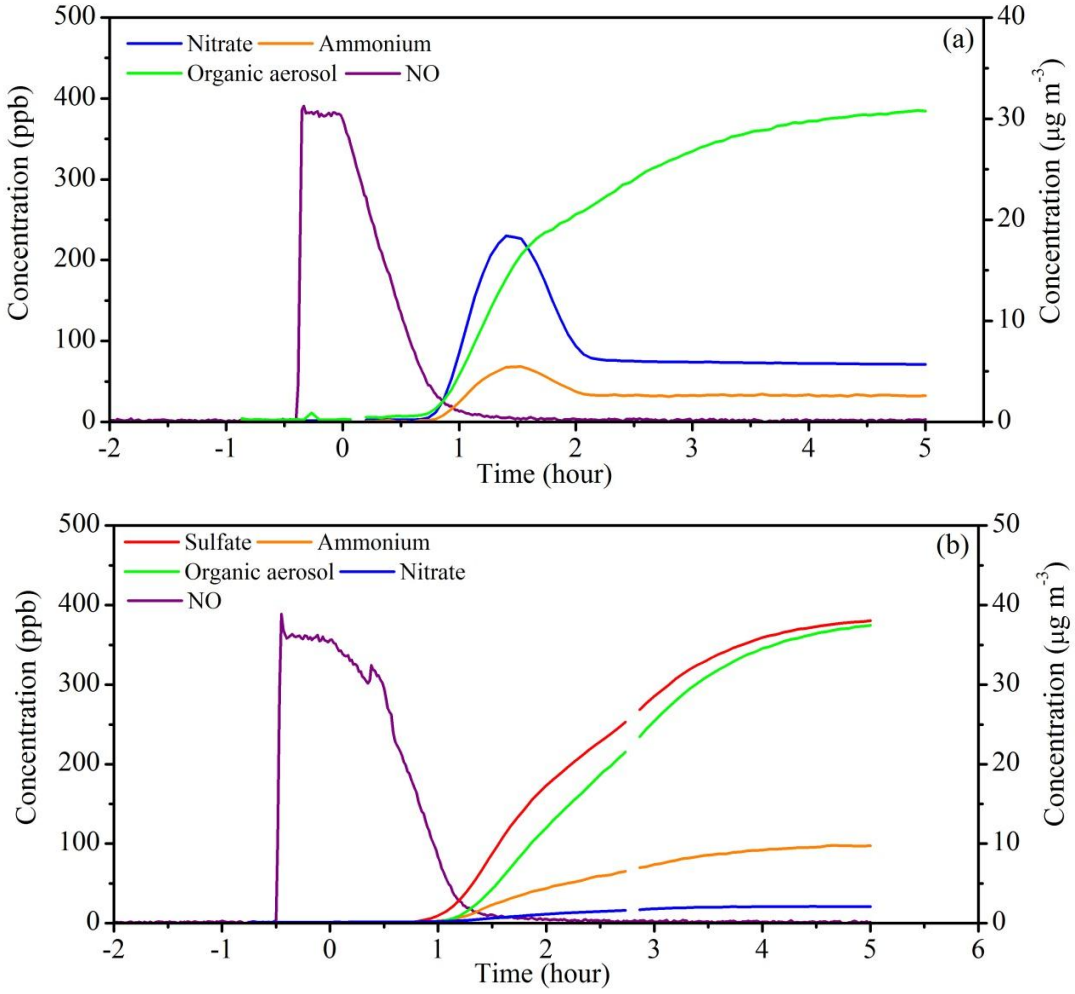


868

869 **Fig. 4**. Concentration–time plots of NO (left-y axis) and particle–phase species
870 (right-y axis) during the photochemical aging of emissions from vehicle II. (a)
871 Without $SO_2$, and (b) with $SO_2$. The concentrations of particle-phase species are
872 wall-loss corrected. At time =0 h, the black lamps were turned on.

873

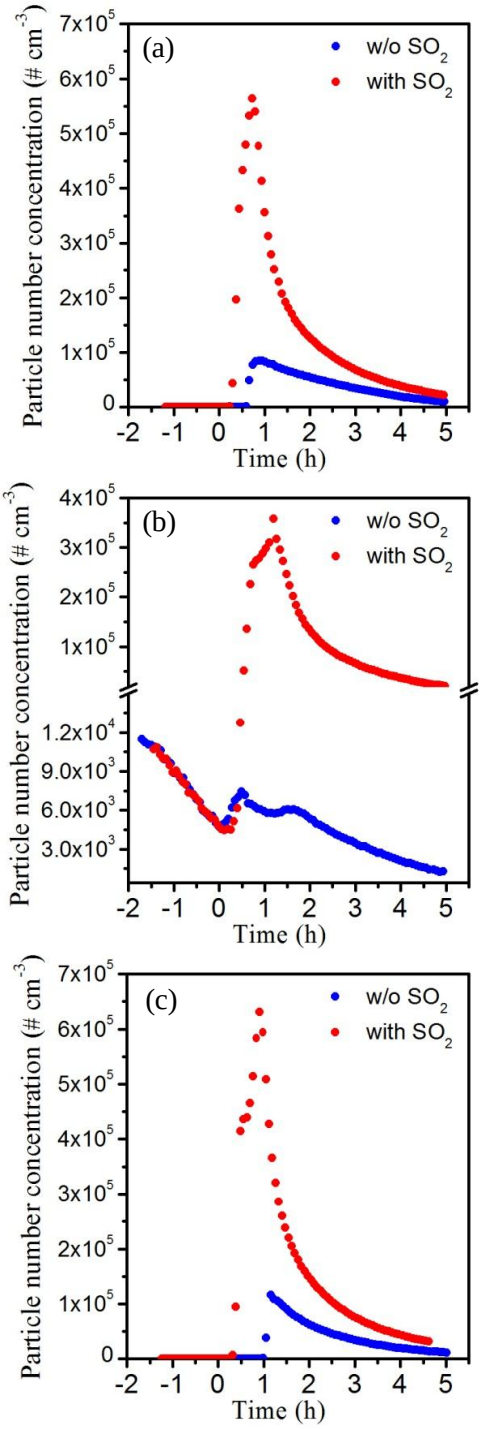


874

875 **Fig. 5**. Evolution of particle number concentrations during the aging experiments of

876 LDGV exhaust for vehicle I (a), II (b) and III (c). At time =0 h, the black lamps were

877 turned on. W/o $SO_2$ and with $SO_2$ in the figures represent experiments without and

878 with adding $SO_2$, respectively.

879

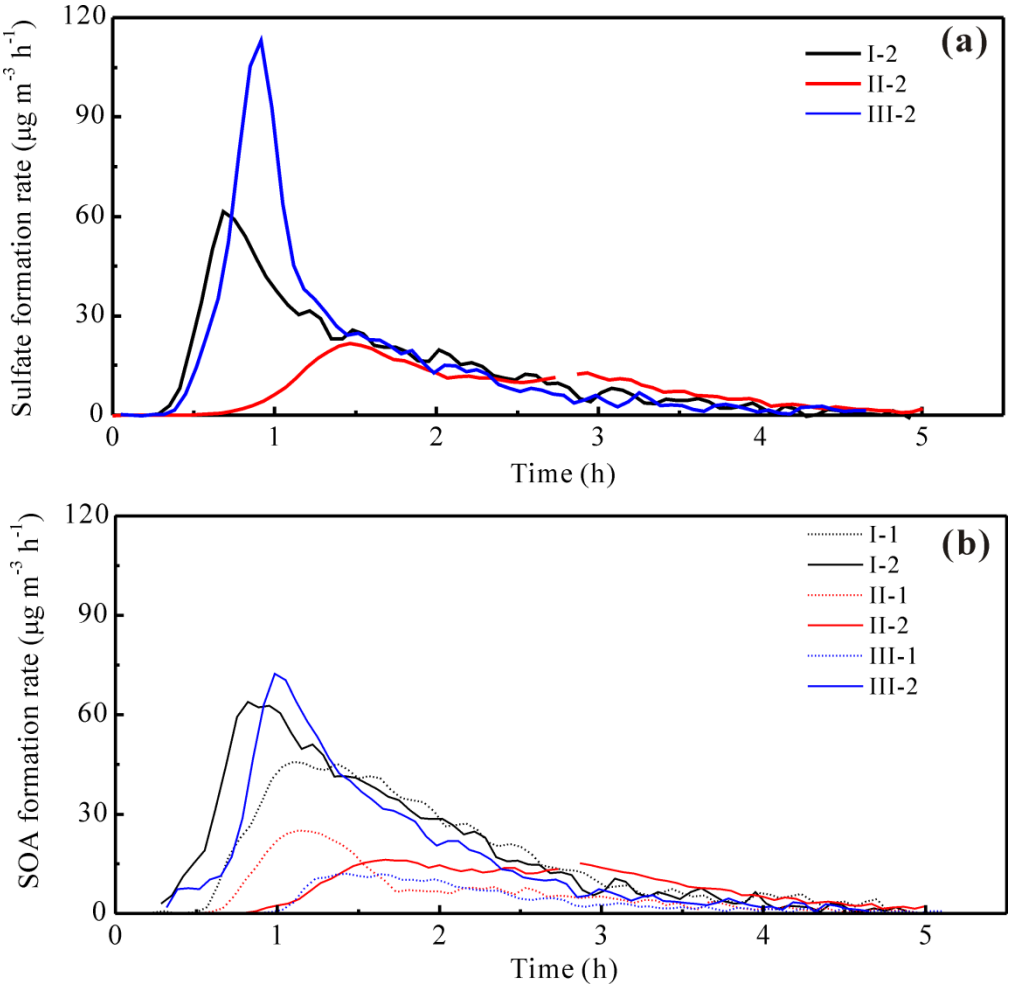


880

881 **Fig. 6.** Sulfate formation rates (**a**) and SOA formation rates (**b**) as a function of time

882 during the photooxidation of LDGV exhaust.

883

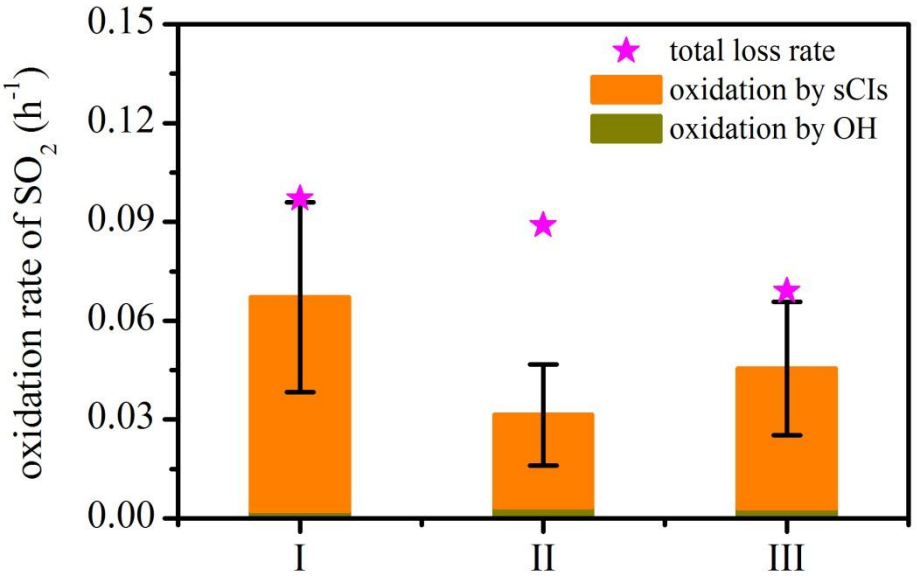


884

885 **Fig. 7.** The oxidation rate of $SO_2$ during the photooxidation of LDGV exhaust with

886 $SO_2$. The loss rates of $SO_2$ reacting with OH radicals and sCIs were calculated by

887 multiplying the reaction rate coefficients derived from the MCM v3.3 by the average

888 OH concentration and estimated sCIs concentration, respectively. Error bars represent

889 the standard derivation (1σ) of the oxidation rate of $SO_2$ by sCIs throughout the whole

890 experiment.

891

892

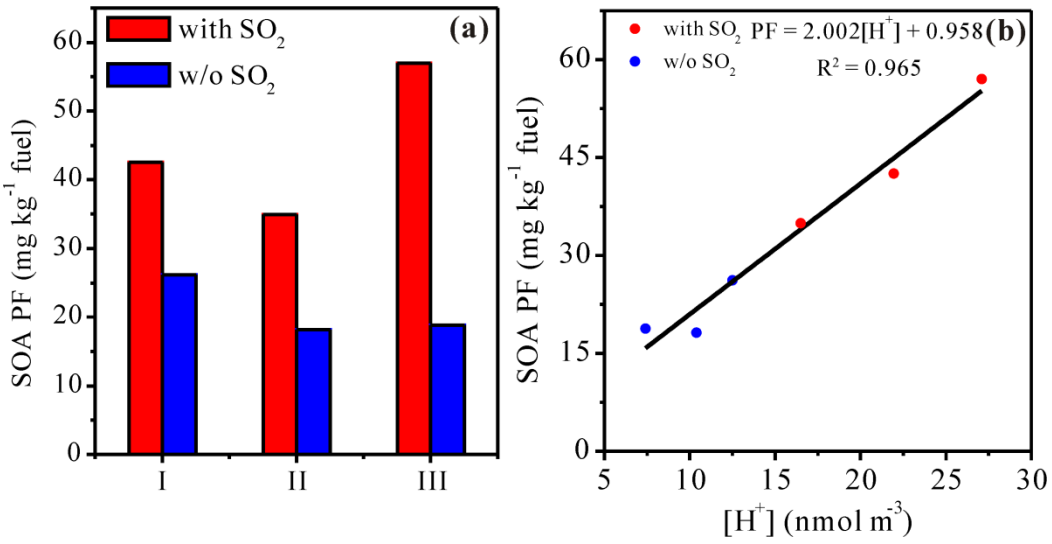


**Fig. 8**. SOA production factor (PF) and its relationship with particle acidity. (**a**) SOA PF after 5 h of photochemical aging of exhaust from different LDGVs with and without additional $SO_2$. (**b**) SOA PF as a function of in-situ particle acidity. The concentration of $H^+$ in particle phase shown here was the value when the SOA formation rate reached the maximum during each experiment.

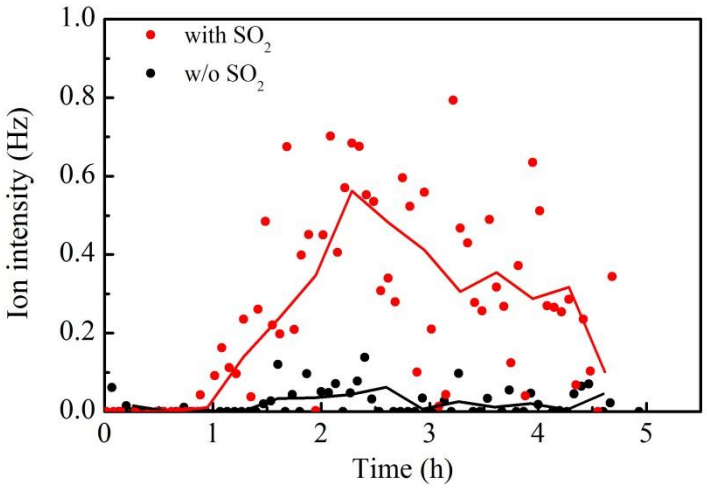


**Fig. 9**. Time evolution of m/z 88 during the aging of LDGV exhaust from vehicle III. Solid lines are derived from the average values of every five data points.

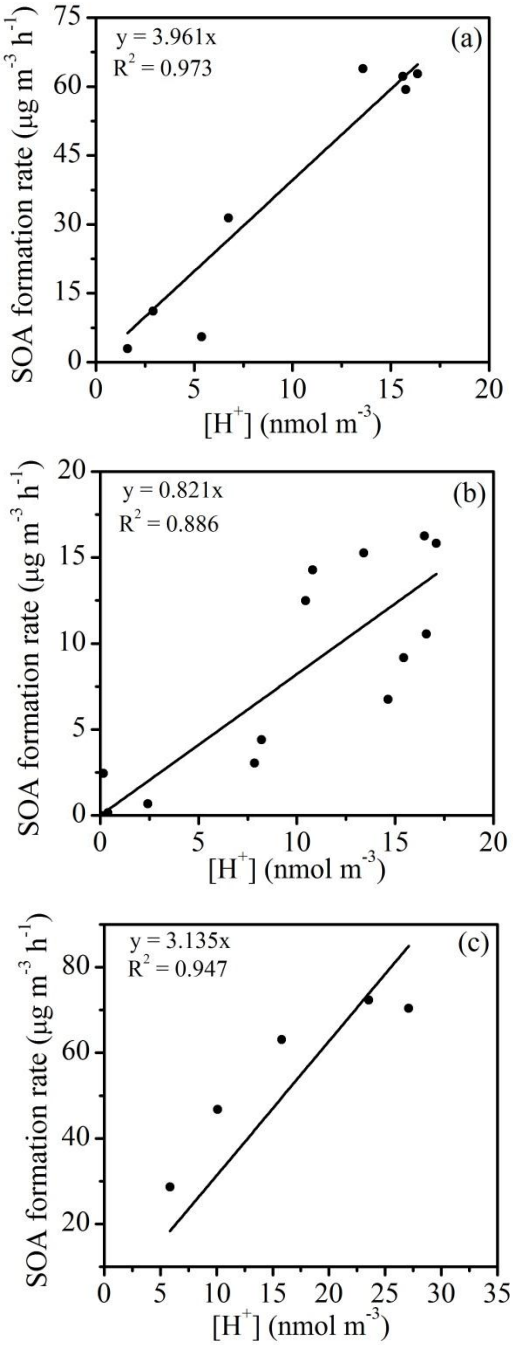


904

905 **Fig. 10.** SOA formation rate as a function of in-situ particle acidity ($[H^+]$) for vehicle

906 I (a), vehicle II (b) and vehicle III (c) with adding $SO_2$. Plotted data were selected

907 from when SOA formation rate was higher than zero to when the rate reached the

908 maximum value.

909

910

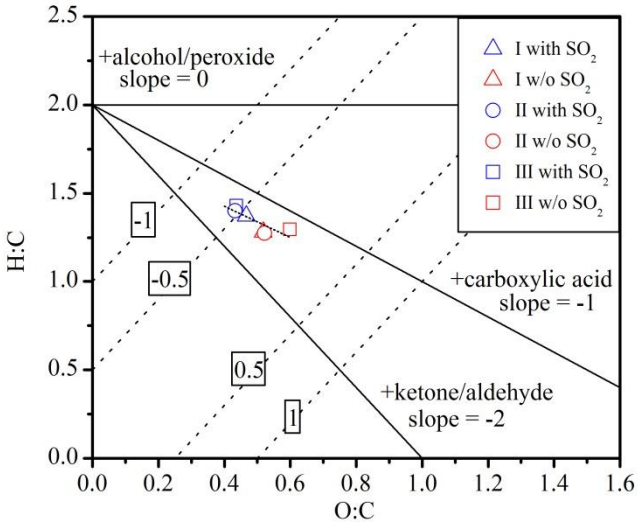


911

912 **Fig. 11.** O:C vs. H:C of SOA formed from LDGV exhaust with and without additional
913 $SO_2$ at the end of each experiment. Blue and red symbols represent data with and
914 without additional $SO_2$, respectively. The dashed lines represent estimated average
915 carbon oxidation states of -1, -0.5, 0.5 and 1 (Kroll et al., 2011). The black lines
916 represent the addition of functional groups to an aliphatic carbon (Heald et al., 2010).